Chapter IV

Results and Discussion

Part A

Design, synthesis and characterization of novel 4-ring achiral bent core liquid crystals by POM, DSC and XRD studies.

4A.1. Introduction

The discovery of spontaneous polarity[1] and chirality[2] in smectic liquid crystals (LCs) of achiral bent shaped molecules has stimulated a new era in soft materials[3] attracting both chemists and physicists alike because of spontaneously chiral and switchable polar phases; polarization splay modulated and layer undulated phases,[4] and the potential applications of these materials in electro-optical devices. The manifestation of nematic phases among the mesophases in materials of bent core molecules is relatively scarce due to strong tendency for smectic layering generated by the close packing of the kinked molecules promoted by aromatic core interactions.[5] Nematic phase is largely realized in derivatives of 1,3-disubstituted phenyl ring with a substituent in 2- or 4- positions.[6] However, reduction of the molecular bent at the apex by the replacement of 1,3-substituted 6-membered phenyl ring by a 2,5-substitued 5-membered heterocycles like oxadiazole,[7] or thiadiazole[7] or unsymmetrical hockey stick molecules[8] or dimesogens comprised of rod-like and bent units[9] (with a overall reduction in bent angle) yielded the nematic phases at high temperatures above the layered smectic or columnar phases. Another modification in the shape of the molecule with a V-shaped central fluorenone unit derivatives possessing apex angle of 90^{O} at the centre also exhibited nematic phases.[10] Hence the realization of nematic phase in bent core molecules is dependent on the molecular architecture with extended aromatic cores and/or relatively shorter terminal chains or reduction of molecular bent promoted by rigid extended five-membered heterocycle ring at the centre.[6]

The *Holy Grail* of liquid crystal science[11] viz., biaxial nematic phase[12-17] (**N_b**) with two optic axes that can be realized in shape based molecules is being explored since four decades by different experimental techniques. In the uniaxial nematic phase the molecular axes are oriented along the director **n**, whereas in the **N_b** phase there is an additional secondary director **m** which is perpendicular to **n** (**Figure. 4A.la and b**).

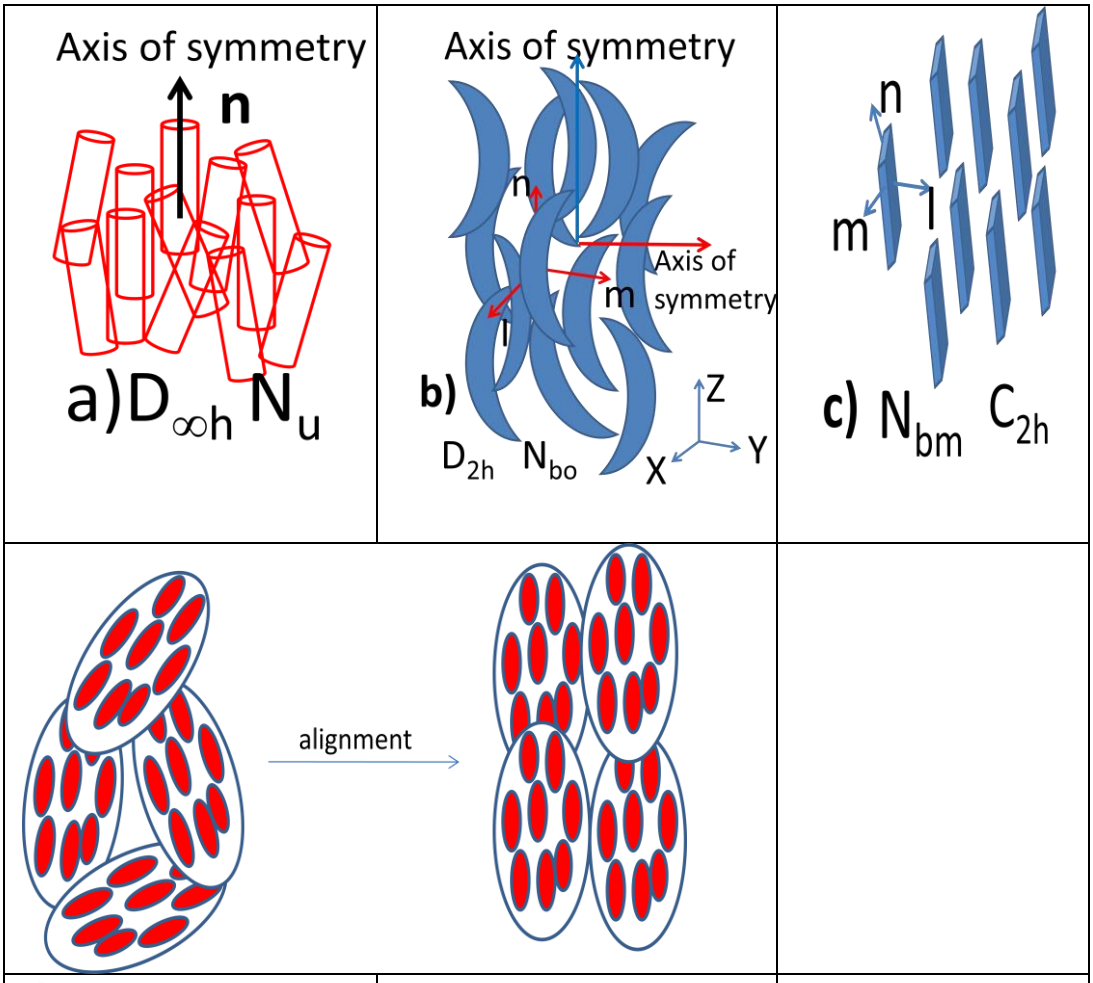

Figure.4A.1 Nematic phases of bent core molecules: (a) unrestricted rotation around the molecular long axis **n** leads to an uniaxial nematic phase(Nu); (b) restricted rotation around **n**, but without polar order, leads to the simplest type of biaxial nematic phase(Nb) with orthorhombic D_{2h} symmetry (N_{bo} phase); (c) biaxial nematic phase with monoclinic C_{2h} symmetry (N_{bm} phase) as for example possible by the organization of the molecules in SmC clusters with frozen rotation around **n**; (d) rotationally disordered biaxial clusters, where the rotational disorder of the clusters around z leads to macroscopic uniaxiality;(e) phase biaxiality due to field or surface- induced or spontaneous alignment of the biaxial clusters.

Bent-core molecules are considered to be one of the potential candidates to realize the thermotropic $\mathbf{N_b}$ phase, even though there is an on-going debate on the existence of the spontaneous biaxial nematic phase in bent-core liquid crystals. The predominant manifestation of two-brush disclinations in the nematic Schlieren texture[18] as primary evidence for the speculation[7a] of biaxial nematic phase in oxadiazole derivatives was supported by the X-ray diffraction patterns[19] with two pairs of diffuse peaks in small angle region. The X-ray

patterns are interpreted[19] based on molecular form factor reflecting molecular shape dependent electron density and structure factor (density-density related to anisotropic short range positional correlations) to explain the biaxiality which is different from classical cybotactic concept.

However similar results of four-spot and two-spot patterns has been reported in a new series of BCMs **1** derived from 4-cyanoresorcinol[6h] with variable length terminal alkyl chains. The results showed that lower homologues of short chain compounds are similar to that exhibited by ordinary calamitic molecules, while the long chain compounds form SmC-type skewed cybotactic clusters[20,21] *i.e.* small regions of space in which molecular centres are arranged in a two-dimensional layered structure, but where the correlation between molecular positions decays very quickly with distance. It has long been known that such short-range correlated "clusters" are possible there even in calamitic liquid crystals, but there they were considered to be important only in pre-transitional fluctuations when approaching a smectic phase. These nematic phases in bent core compounds can be regarded as strongly fragmented SmC type phases.

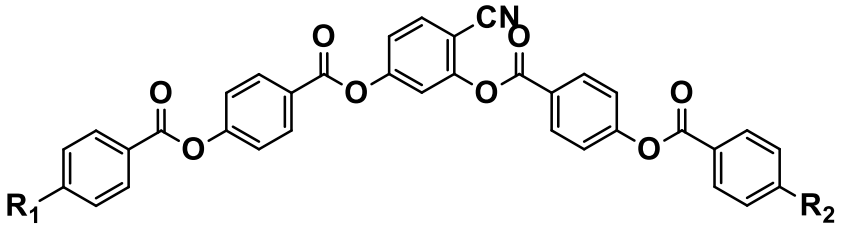

1: 4-cyanoresorcinol derivatives, R1 and R2 alkyl/oxy chains

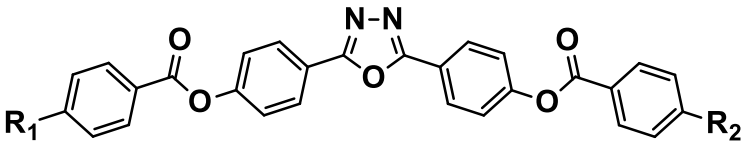

2: 2,5-bis(p-hydroxyphenyl)-1,3,4-oxadiazole (ODBP) derivatives

However recent results[22-24] on bent core molecules derived from 2,5-bis(p-hydroxyphenyl)-1,3,4-oxadiazole (ODBP) **2,** exhibiting nematic phase with a signature of small angle four-spot X-ray diffraction pattern confirm the existence of short range cybotactic clusters.[21] Interestingly X-ray diffraction small angle four-spot pattern in low temperature region evidenced[22-24] the cluster

formation of skewed cybotactic supramolecular structure with temperature dependent tilt angle. High resolution X-ray studies confirmed the presence of cybotactic clusters of SmC like ordering in low temperature region in lower homologue of ODBP exhibiting nematic phase only. Further the two-spot pattern in high temperature region of the nematic phase is similar to that of the uniaxial N phase of conventional calamitic molecules. Polarizing Optical Microscopy (POM) studies[25] evidenced the biaxial nematic to uniaxial nematic phase transition (in ODBP derivative with C7 homologue) confirming the signature of four-spot to two-spot pattern[24] in X-ray studies.

Recently we reported the fluid smectic LC phases with spontaneously growing chiral and polar layers (SmCP phases) including the polarization splay modulated and layer undulated (PMLU) $B_7/B_{1Rev/Tilted}$ phases variants in four ring bent coresystems.[26] The four ring molecule possesses two OH groups in two wings, located in unsymmetrical positions, which deviates significantly from the typical symmetrical and/or V-shape of other bent core molecules. Further we observed helical structures in these four ring achiral systems and this phenomenon is the strong evidence that the origin of the chirality in this system viz. ferro/antiferroelectricity and twisted structures is related to the twist conformation of these molecules. The modification of angular 3,4$^{/}$-disubstituted biphenyl unit[27] with the introduction of an ester linkage viz., COO moiety between the phenyl units, reduction of phenyl rings and proper choice of a substituent and its position in the central core leads to structural variation of polar groups in bent core molecules and hence can promote a broad range of interesting variations[26] in their mesogenic properties. Any substituent ortho to ester linkage separating the two phenyl rings may substantially change the conformation of the molecule depending on the size, polarity and direction of substituents and hence can contribute to the formation of novel phases. As a part of our work on four ring bent core systems we modified the central core with the introduction of methyl substituent in the bay position of the central bent core. Further the four-ring molecule possess an unequal distribution of aromatic rings in the two wings which manifest the unsymmetrical bent shaped molecule and hence can be regarded as a true hockey stick molecule bordering the bent core and calamitic

molecules. Here we report the first observation of a new phase variant viz., classical nematic (**N)**-cybotactic nematic ($\mathbf{N_{cyb}}$)-coexistent cybotactic SmC-SmA cluster-SmA exhibited by an achiral four ring bent core system with the help of polarizing optical microscopy (POM), differential scanning calorimetry (DSC) and X-ray diffraction (XRD) studies.

4A.2. Experimental:

The starting material in the present study 4-n-alkyloxysalicylaldehyde was prepared by Williamson etherification of 2,4-dihydroxybenzaldehyde with appropriate n-alkyl bromide. 2-methyl,3-nitrobenzoic acid was converted into corresponding amine by reduction using 10% Pd-C, which was condensed with 4-n-alkoxy salicylaldehyde in presence of few drops of glacial acetic acid. On the other hand,4-decyloxy)phenyl)diazenyl)phenol was prepared by diazonium coupling reaction using 4-n-decyloxy aniline; which was further subjected to esterification reaction to yield the target compound. The compounds were further recrystallized repeatedly to get the pure samples. The formation of all of the compounds was confirmed by ^{1}H-NMR and IR spectroscopy and the purity was established by elemental analysis. The other homologues with n = 4,5,10, 11, 12, 13, 14,16 and 18 were also synthesized following the same procedure and characterized. The details of the experimental procedures along with the spectroscopic data for all the homologous series of compounds are presented in the experimental part of **Chapter III**. The liquid-crystalline behaviour of the synthesised compounds had been investigated by optical microscopy and differential scanning calorimetry (DSC).

4A.3. Results and Discussion:

4A.3.1. POM and DSC studies:

The four ring system consists of three different types of linkage units (azo -N=N-, ester -COO-, and salicylidene –CH(-C-OH)=N-) bridging the phenyl rings to each other. The molecular structure and the associated thermodynamic data of the phase transitions of the first example of achiral four ring asymmetric bent-core compounds of 2,6-disubstitued toluene derivatives **12-10** exhibiting thermotropic

nematic-SmA-like phases are shown in **Scheme 1** and **Table4A.3.1** respectively. The synthetic details of the compounds are presented in **Scheme 1**.

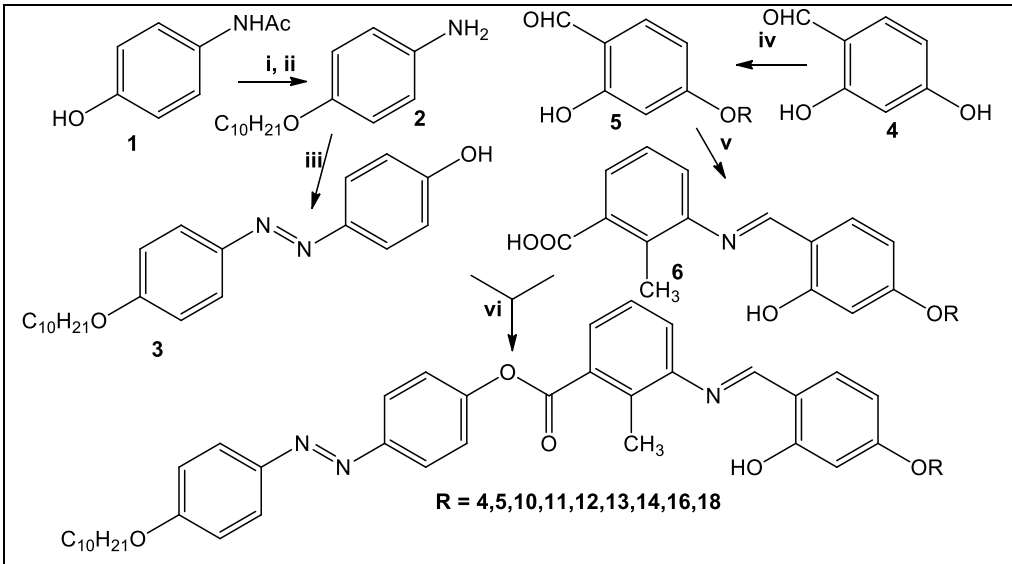

Scheme 1: Synthetic details of the compounds 1a and 1b, Reagents and conditions: i. dry acetone, K_2CO_3, $C_{10}H_{21}Br$, KI, Reflux, 24h; ii. H+, H_2O, OH-, H_2O; iii. HCl, $NaNO_2$, 0-5^{0}C,Phenol, NaOH; iv. dry acetone, $NaHCO_3$, $C_nH2_{n+1}Br$; v. 2-methyl-3-aminobenzoicacid, Abs EtOH, AcOH, reflux, 6h; vi. DCC, DMAP, DCM, Stirring 48h

Table4A.3.1: Phase transition temperatures (^{0}C) of the compounds, recorded for second heating (first row) and second cooling (second row) cycles at 5^{0}C/min from DSC. The enthalpies (ΔH in kJ/mol) and entropies (ΔS in J/mol/K) respectively are presented in parentheses.

Compound	**K- SmA**	**SmA-N**	**N-I**
18-10	120.8(34.0, 86.5)	134.0(1.23, 3.03)	139.9(0.55, 1.33)
	102.2(29.7, 79.1)	132.1(0.93, 2.31)	139.1(0.42, 1.03)
16-10	122.1 (38.3, 97.0)	133.3 (1.17, 2.8)	143.1 (0.43, 1.04)
	102.0 (33.9, 90.5)	132.1 (0.97, 2.4)	142.3 (0.43, 1.04)
14-10	120.3 (40.3, 102.6)	127.6 (0.96, 2.41)	143.2 (0.5, 1.2)
	92.7 (35.7, 97.8)	124.4 (0.48, 1.21)	141.0 (0.28, 0.68)

13-10	121.1(31.76, 80.5)	126.9 (0.69, 1.72)	147.4 (0.32, 0.75)
	94.2 (27.2, 74.2)	123.8 (0.55, 1.39)	145.5 (0.16, 0.38)
12-10	119.3(35.6, 90.8)	122.3(0.73, 1.84)	149.2(0.43, 1.02)
	92.9(32.5, 88.8)	121.8(0.84, 2.13)	148.9(0.51, 1.21)
11-10	115.6 (33.1, 85.3)	117.2 (0.2, 0.6)	150.2 (0.4, 1.1)
	90.5 (28.2, 77.7)	114.5 (0.5, 1.47)	148.6 (0.3, 0.7)
10-10	109.3 (40.8, 104.6)	115.8 (40.4, 104.0)	151.6 (0.49, 1.15)
	89.6 (31.9, 88.0)	106.5 (0.5, 1.32)	150.5 (0.49, 1.2)

The compound exhibits **12-10** broad mesomorphic range with clearing temperatures below 150^0C. The DSC spectrum for **12-10** is shown in **Figure4A. 3.1.2**.

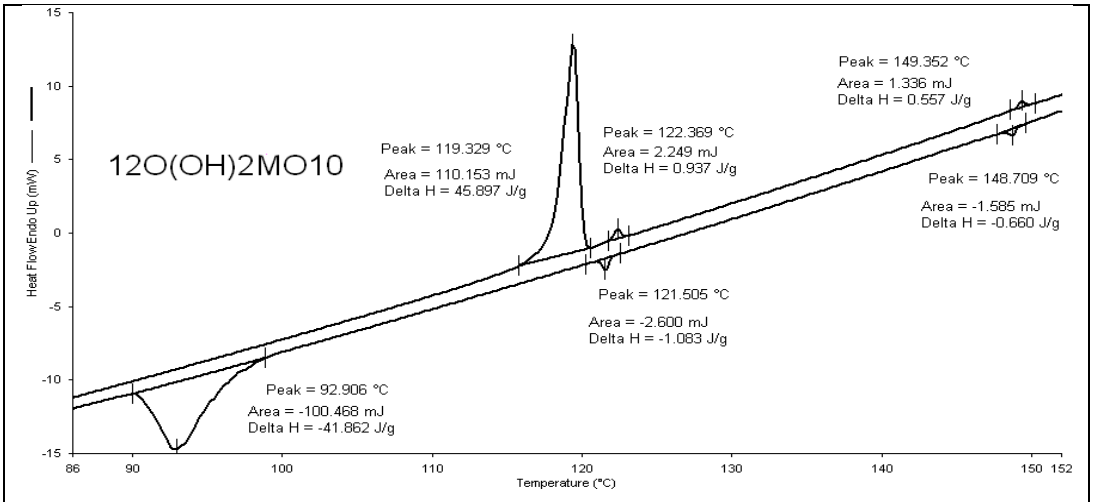

Figure4A. 3.1. 2: DSC spectrum of **12-10** recorded in the second heating/cooling cycle at @ 5^0C/minute.

The optical textures of sample **12-10** using four different preparation methods (i) untreated glass plate and coverslip (ii) nylon-66 treated glass plate and coverslip (iii) aligned planar cell and (iv) homeotropic cell are studied. The examination of

the pristine samples for **12-10** sandwiched between a untreated slide and a coverslip gave usual and unusual textures when examined on **POM** attached with a hot stage, which are shown in **Figure 4A. 3.1.3.** **12-10** on cooling from the isotropic phase exhibited distinctly well known characteristic textures of nematic phase viz. 2- and 4-brush Schlieren texture, planar and marble textures with threads as boundaries throughout the nematic phase temperature range. The growth of Schlieren texture is accompanied by Brownian motion. The lower temperature phase exhibited unknown *SmA* like phase characteristic features which are different from calamitic SmA phases. The organisation of molecules in schlierien brush is shown in **Figure 4A. 3.1.3(e)** and **(f)**.

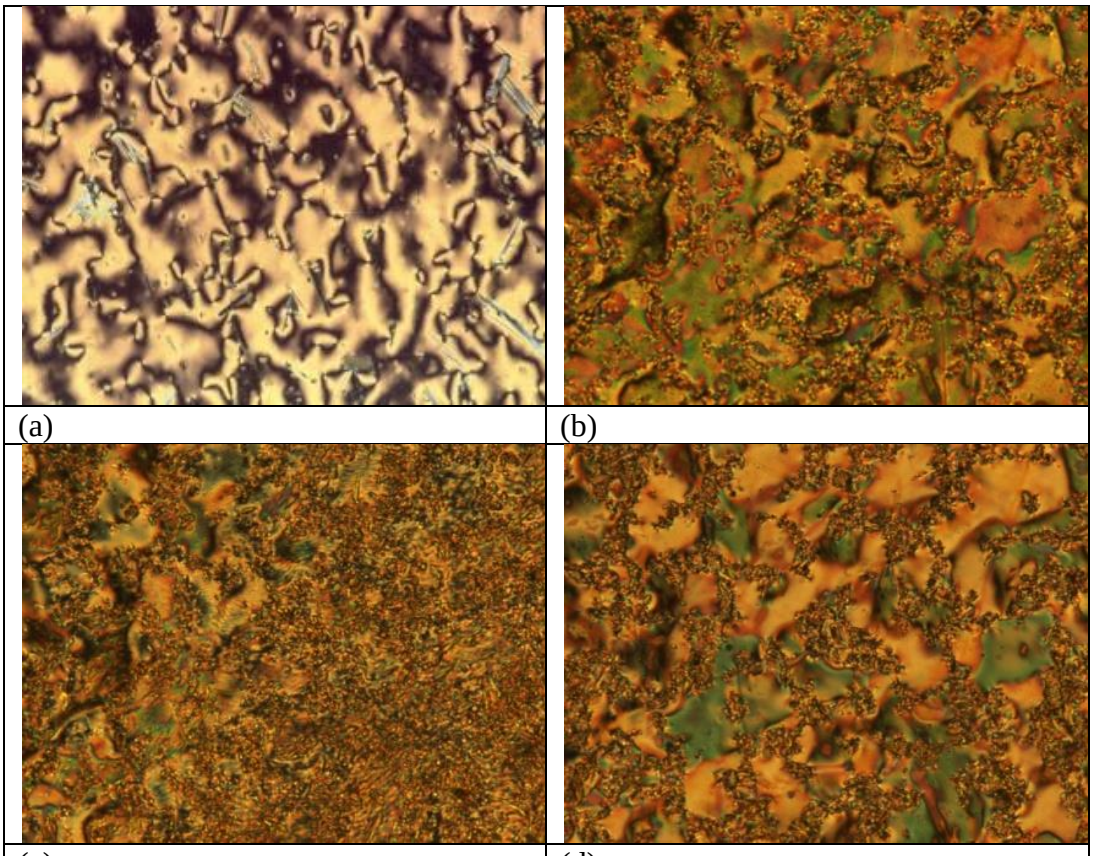

Figure 4A.3.1.3: Defect texture of the nematic phase of compound **12-10** on cooling from isotropic phase (a) majority 2-brush defect texture at 147^0C (b) at 145^0C at different site (c) during nematic- another mesomorphic phase transition at 121.8 ^{0}C (d) at 120.5^0C on a untreated glass slide and coverslip.

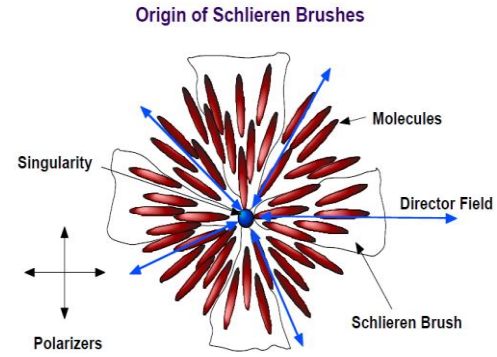

(e)

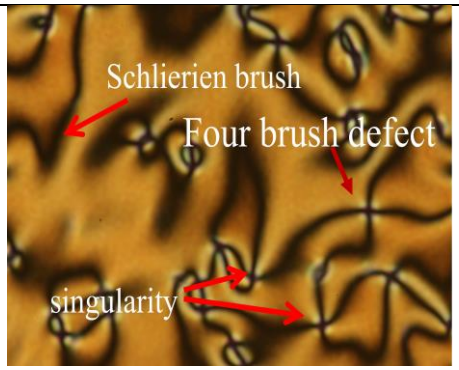

(f)

12-10 exhibited marble textures with threads in nylon-66 treated glass plates **(Figure 4A. 3.1.4a)**. On further cooling, the sample undergoes a phase transition from the stable nematic phase (N) spreading with ripples in the entire field of view over a period of time as shown in **Figure 4A. 3.1.4b** during transition to fluid *SmA* like mesophase exhibiting a birefringent planar domain texture with well defined boundaries. The transition from N-SmA like phase is accompanied by transient Schlierien texture with undulation lines. These undulation lines /fingerprint texture is stable and do not disappear over a period of time and temperature. The flow of such undulations started growing within each domain, subsequently disappeared on further cooling and developed into distinctly different dark and bright adjacent domains with walls separating one domain from another.

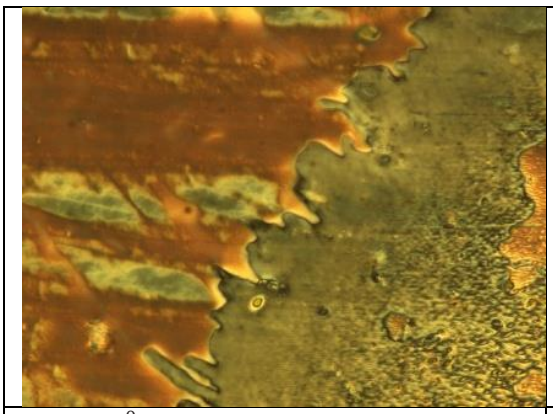

(a)122.2^{0}C

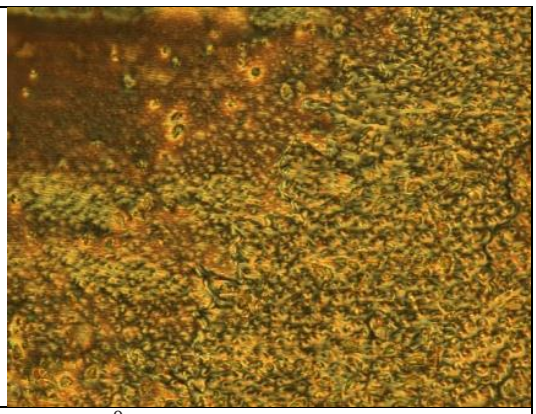

(b)122.2^{0}C after 1m

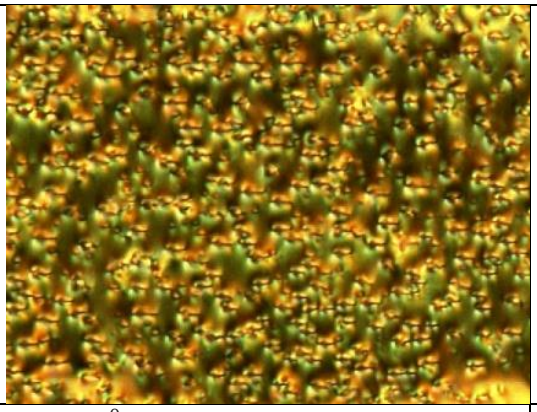

(c)122.1^{0}C after 10 m

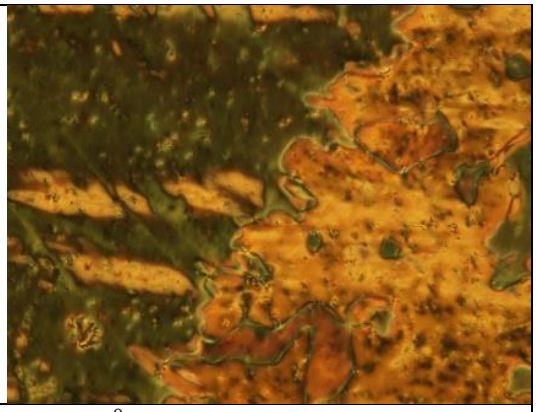

(d)122.0^{0}C

Figure 4A.3.1.4: The phase transformation from N-another mesomorphic phase is accompanied by ripples which slowly spreads over a period of time indicating the segregation of molecular assemblies followed by organization in adjacent domains

The same finger-print texture or undulation lines are also observed in homeotropic cells with alignment layers like (i) Silane coupling, (ii) Cytope, (iii) SE-1211 and (iv) JALS-204 on transition from nematic to smectic phases as illustrated in **Figure 4A. 3.1.5.**

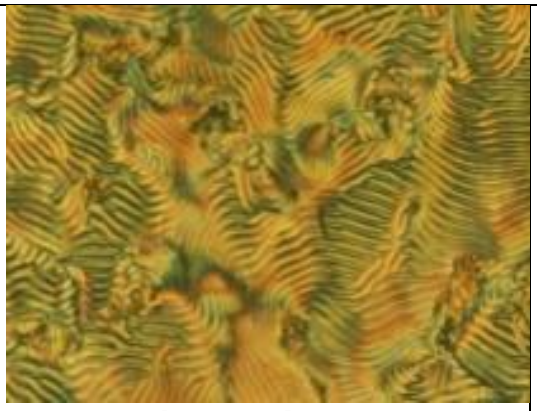

(i) Silane coupling

(ii) Cytope treated

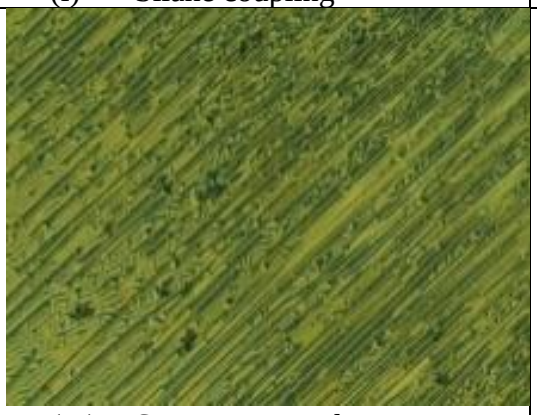

(iii) SE-1211 treated

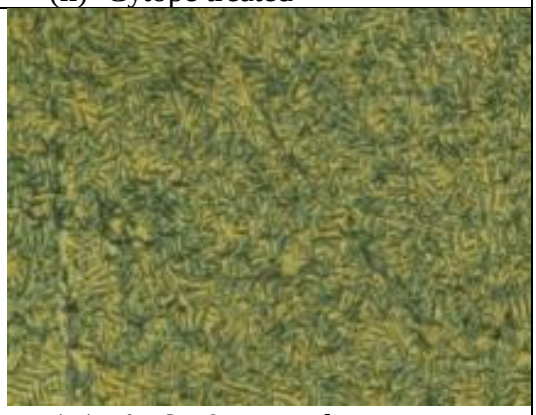

(iv) JALS-204 treated

Figure 4A. 3.1.5: Finger-print texture or undulation lines in cells with different reagents treated for hometropic alignment.

In a commercial PI coated parallel rubbed sandwich cell filled with the sample **12-10, c**hange in birefringence with decreasing temperature when the stage of sample **12-10** in extinction position was rotated by 10^{O} from crossed polarizers. The birefringence in high temperature phase increased with the decreasing temperature (**Figure 4A. 3.1.6**).

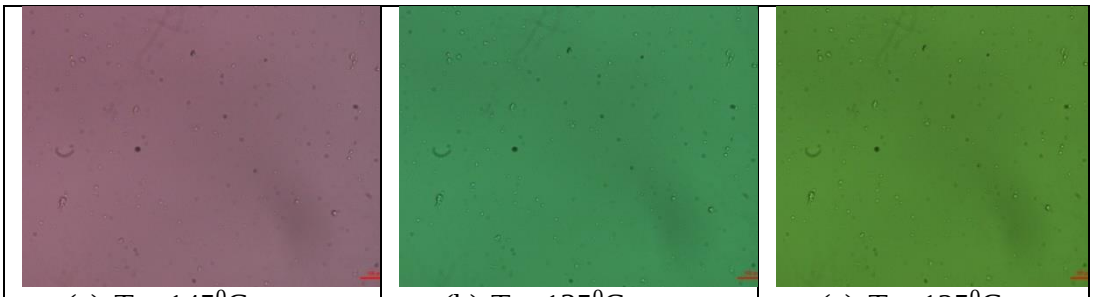

(a) T = 145^{0}C (b) T = 135^{0}C (c) T = 125^{0}C

Figure 4A. 3.1.6: Change in birefringence with decreasing temperature when the stage of sample **12-10** in extinction position was rotated by 10^{0} from crossed polarizers.

The low birefringence in the PI coated cell can be explained due to a small film thickness of approximately 5.0 μm. In bent core compounds even though uniaxial and biaxial nematic phases are observed, very few reports on chiral nematic phases appeared in literature.[6d, 6e,7d, 7e, 28]. However when the director (optic axis) of the nematic phase was aligned with one of the polarizer's direction in POM studies, the sample appeared black **Figure 4A. 3.1.7a**, a defect free planar texture, such that the high temperature phase resembled a birefringent plate of a crystal with the optic axis in the plane of the substrate. With the variation of the sample in azimuthal angle the transmitted light intensity between crossed polarisers continuously increased to a maximum (**Figure 4A. 3.1.7b),** when the optic axis was oriented at 45^{O}. The nematic phase was confirmed by characteristic flickering upon tapping the sample caused by Brownian motion. On further cooling the nematic phase transformed into another mesomorphic phase by a very slow growth of two types of spiral textures (**Figure 4A. 3.1.7c)** of opposite twist resembling the filament textures of B7 phase or knitting instability, which later transformed into cluster like regions with complimentary colours in adjacent domains and with a strong increase in birefringence as shown in **Figure 4A. 3.1.8a-e**. Photomicrographs of the sample **12-10** in a planar cell oriented for

maximum extinction of the domains in the lower temperature *SmA* like phase (a) in crossed polariser and analyser arrangement (b) polarizer rotated clockwise 10^{O} (c) polarizer rotated anticlockwise 10^{O}, (d) sample rotated clockwise 10^{O} and (e) sample rotated anticlockwise 10^{O} are shown in **Figure 4A. 3.1.8a-e.**

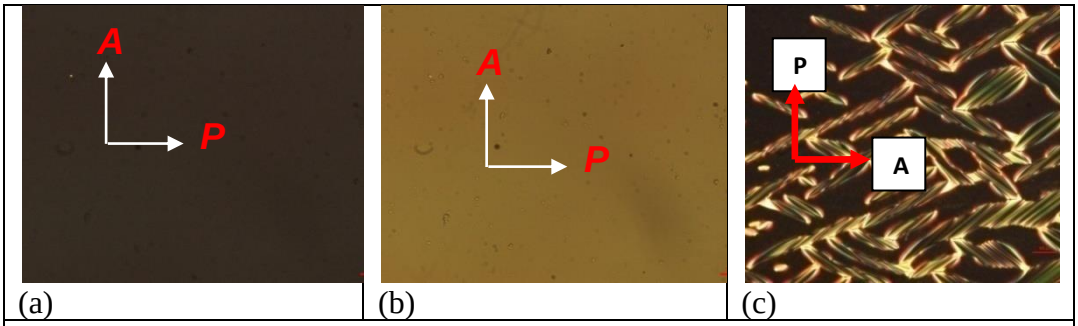

(a) (b) (c)

Figure 4A. 3.1.7 (a) texture of director orientation of a uniform planar uniaxial nematic phase between crossed polarizers in extinction position and (b) maximum transmittance at 45^{0} with respect to polarizer/analyzer (c) growth of two types of adjacent spiral regions during phase transformation at 125 ^{o}C.

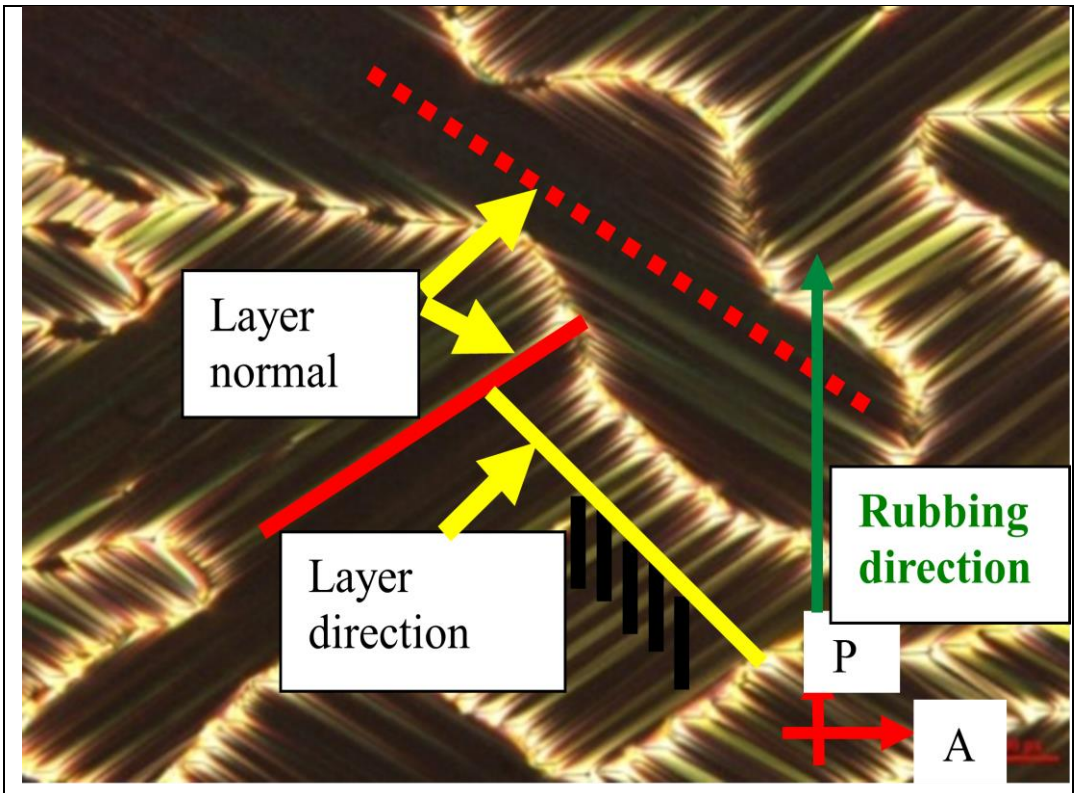

(a) 110.5^{0}C 20m

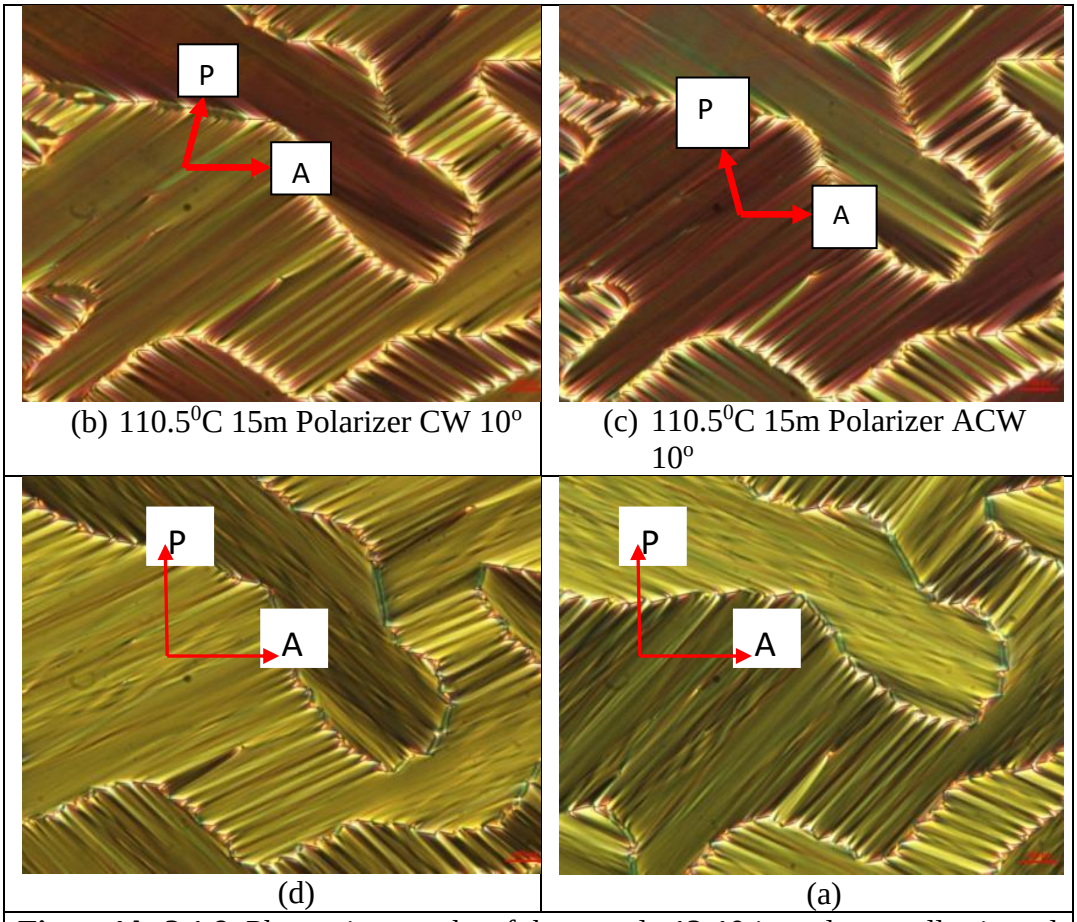

(b) 110.5^{0}C 15m Polarizer CW 10^o (c) 110.5^{0}C 15m Polarizer ACW 10^o

(d) (a)

Figure4A. 3.1.8: Photomicrographs of the sample **12-10** in a planar cell oriented for (a) maximum extinction of the domains in the lower temperature Smectic like phase Stable adjacent regions of complimentary colours and stripes with fluidity. (b) polarizer rotated clockwise (c) polarizer rotated anticlockwise (d) sample rotated clockwise 10^0 and (e) anticlockwise 10^0. The distinct regions are appearing identical and the difference in orientation of the molecular arrangement in each domain indicates the molecular alignment either parallel or perpendicular to the polarizer respectively

There is a difference in orientation of the molecular arrangement in each domain which indicates the molecular alignment either parallel or perpendicular to the polarizer respectively. There is occurrence of dark and bright regions when the sample is rotated between crossed polarisers and hence it is apparent that the orientation of the layer direction is perpendicular to the stripes (as usually observed for SmC phases). The stripe patterns and the orientation of the stripes are the distinct characteristics of the banana shaped molecules and they differ from the conventional SmA or SmA* phase.

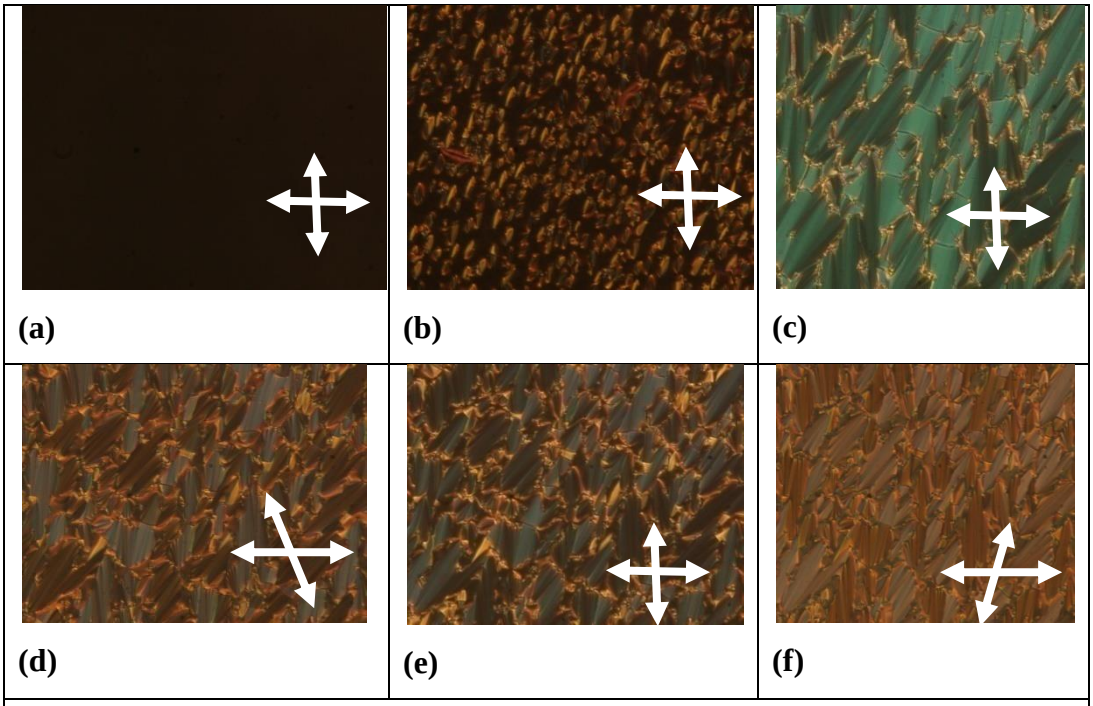

Figure 4A. 3.1.9 (a) texture of director orientation of a uniform planar uniaxial nematic phase of **18-10** between crossed polarizers in extinction position at 136^{o}C, (b) growth of two types of adjacent spiral regions during phase transformation at 130 ^{o}C,(c) smecticA like phase at 115 ^{o}C,(d) polariser rotated anti-clockwise at 120^{o}C (e) Stable adjacent regions of complimentary colours and stripes with fluidity at 120^{o}C, (f) polariser rotated clockwise at 120^{o}C.

4A.3.2. X-Ray diffraction (XRD) investigations of magnetically aligned samples:

XRD was carried out in the nematic phase of compound **12-10**, oriented in a magnetic field of strength (**B = 0.386 T**, cooling rate 0.5 ^{O}C·min^{-1}). **Figure4A.3.2 10** shows the 2D small-angle X-ray scattering (SAXS) patterns of magnetically aligned sample of **12-10** at different temperatures. On cooling the sample in a planar cell, from the isotropic phase below T = 148^{O}C, we see phase-1 (**Figure4A.3.1.3a**), which shows Schlieren textures with mainly 2-brush defects between untreated glass plates and possesses thermal fluctuations, characteristic of a uniaxial nematic phase. In a homeotropic alignment of the sample, this phase does not appear completely dark under crossed polarisers, indicative of a biaxial or tilting molecular arrangement.

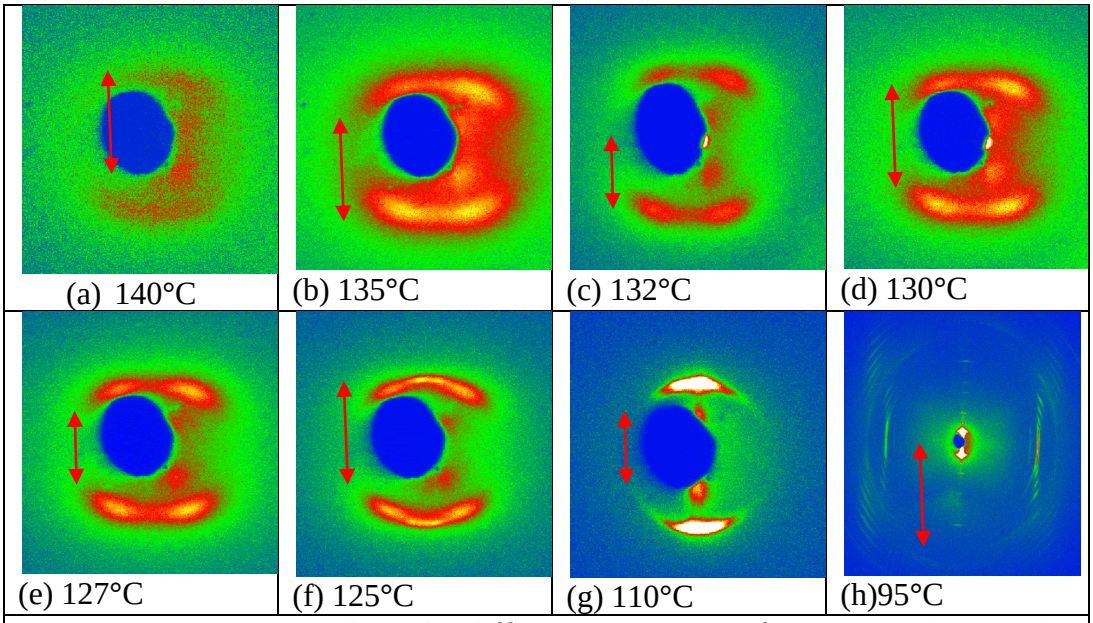

Figure 4A.3.2.10: Small angle diffraction patterns of magnetically samples (direction of magnetic field, **B** is shown as red arrow) in the nematic and smectic phases of compound **12-10** at temperatures (a) 140°C,(b) 135°C,(c) 132°C ,(d) 130°C , (e) 127°C , (f) 125 °C (g) 110°C and (h) wide angle scattering at 95°C **.**

In the XRD study at T=140^{O}C (phase-1), the SAXS pattern as shown in Figure 10a are centered on the equator indicating a fluid nematic phase. Cooling the sample to 135^{0}C, a change in diffuse SAXS pattern with clear maxima besides the meridian resembling a dumb bell shape as shown in **Figure4A.3.2.10b** reflects different molecular alignment. The intensity of the SAXS is significantly higher than that of the diffuse wide angle scattering (**Figure 4A.3.2.11**).

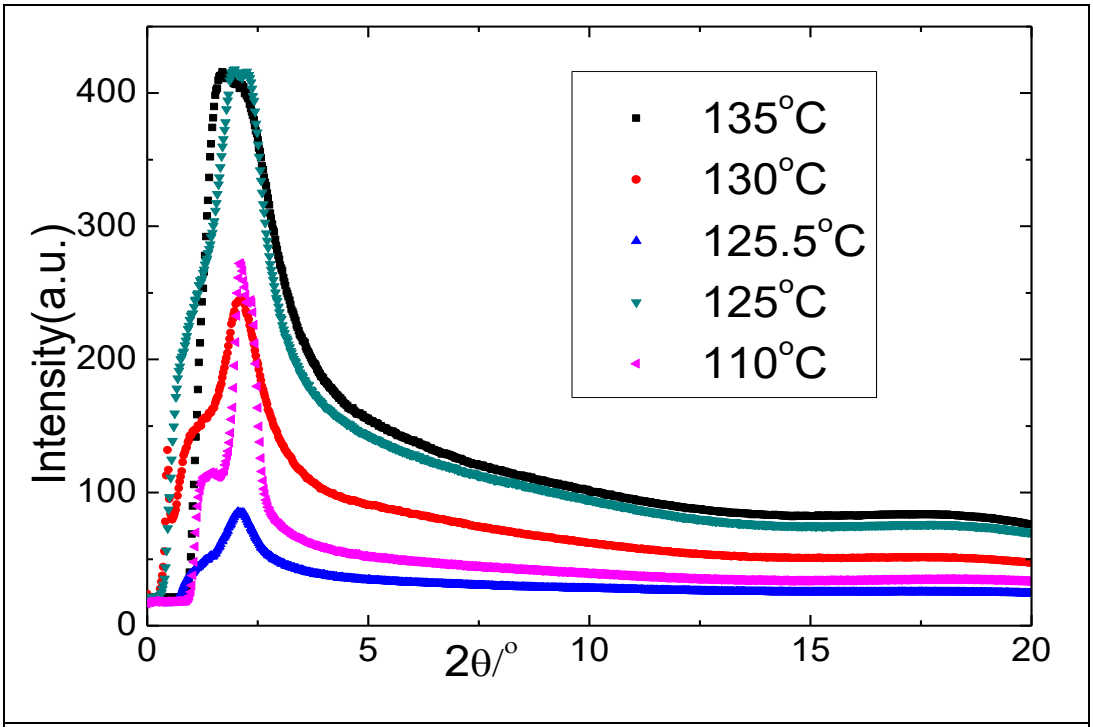

Figure 4A.3.2.11: 2θ-scans over the small and wide angle scatterings at temperatures 135^{0}C, 130^{0}C, 125.5^{0}C, 125^{0}C and 110^{0}C.

In this case the χ-scans over the small angle regions clearly indicated four symmetrically located diffuse maxima (**Figure4A.3.2.12a**) with a tilt angle (~13^o) and the 2θ scan in SAXS pattern (**Figure4A.3.2.11**) gave the maximum at d = 41.0 Å. The experimental 'd' value is smaller than the molecular length of 42.1 Å as evidenced from the energetically optimised preferred molecular structure of **12-10** shown in **Figure4A.3.2.13** in gaseous phase which was obtained from density functional theory studies at the B3LYP/6-31G(d) level basis set performed using ground state restricted *ab initio* Hartree-Fock calculations. Calculated bend angle is 149^0.

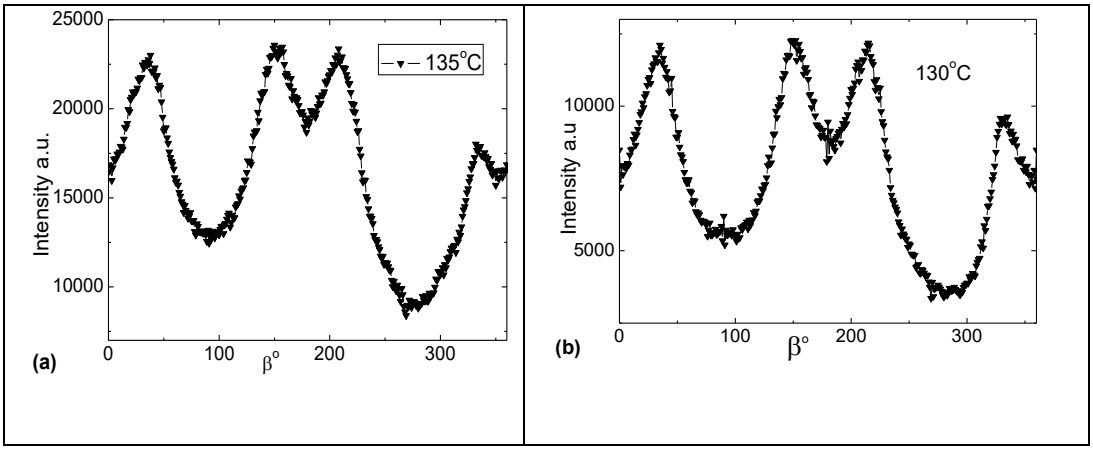

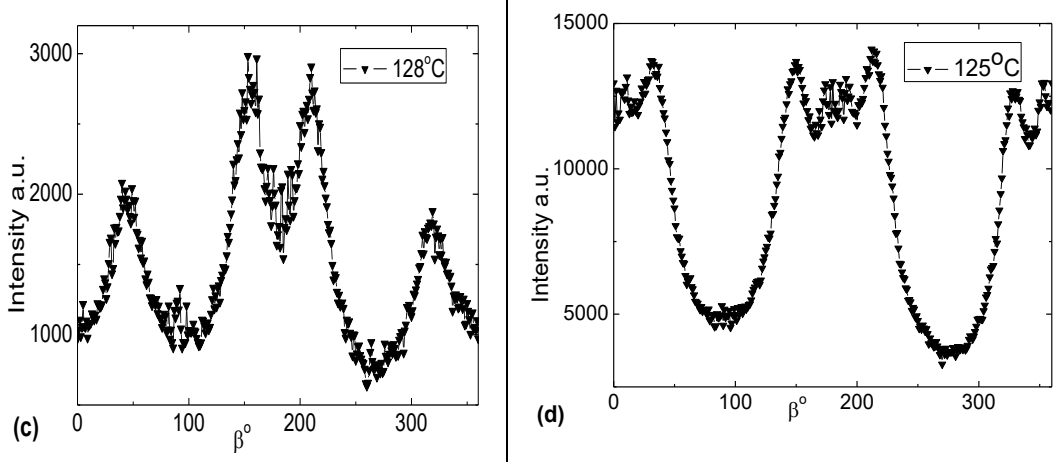

Figure4A.3.2. 12: χ-scans over the small angle regions for **12-10** at temperatures 135^{0}C, 130^{0}C, 128^{0}C and 125^{0}C.

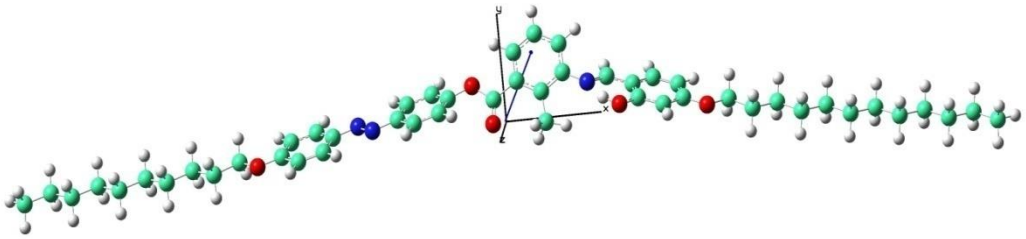

Figure4A.3.2. 13: Optimised molecular structure of **12-10.**

Temperature variation of 2θ scan as a function of intensity in small angle region confirms different molecular arrangements in lower and higher temperature regions of the nematic phase. The SAXS pattern in the region 125~135ºC, shown in **Figure4A.3.2.14**, confirmed molecular arrangement resembling SmC type cybotactic clusters (hereafter abbreviated as **N_{cybC})**, different from that of molecular arrangement of classical nematic phase in high temperature region >135ºC.

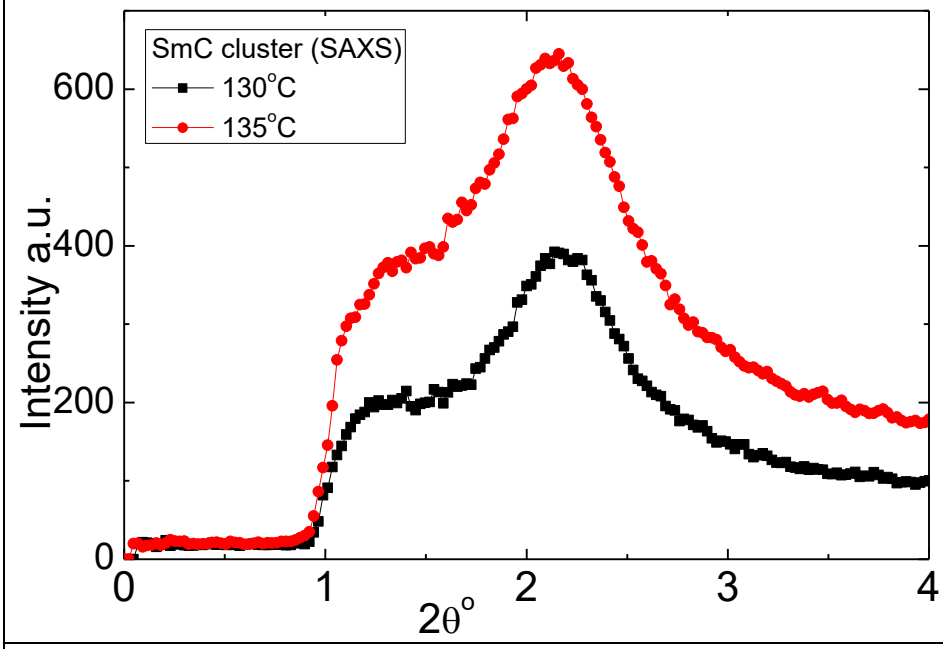

Figure 4A.3.2.14: Smectic C cluster in the small angle diffraction**.**

The organisation of molecules in a cybotactic nematic phase with SmC type clusters ($\mathbf{N_{cybC}}$) aligned under a magnetic field **B** parallel to the molecular long axis is shown in **Figure4A.3.2.15**.

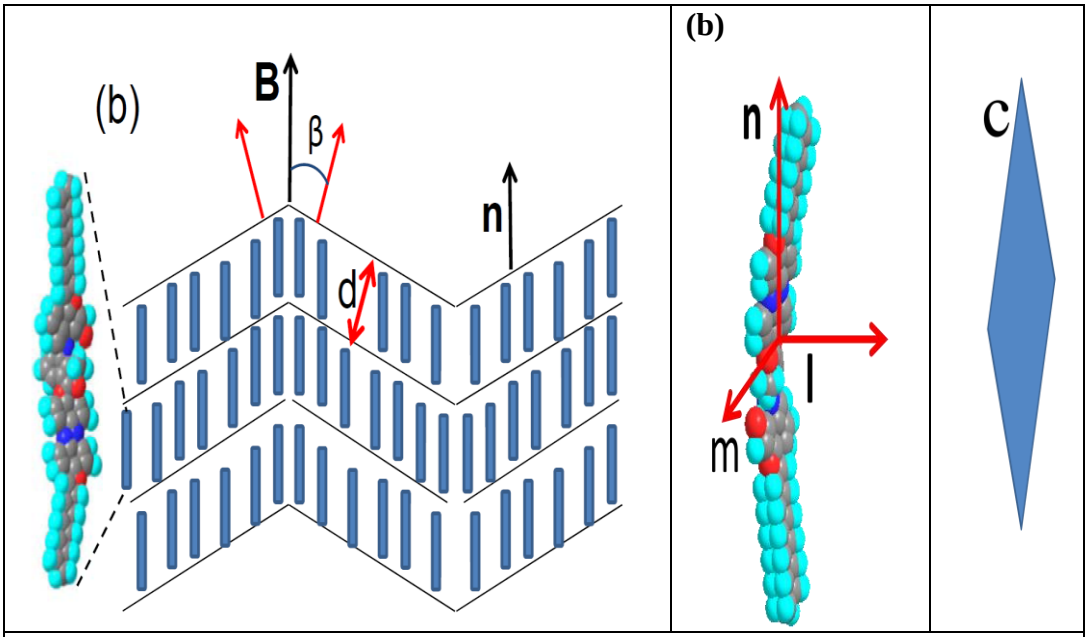

Figure 4A.3.2.15: Organisation of the molecules in a skewed cybotactic nematic phase (N_{cybC} phase) aligned under a magnetic field B parallel to the molecular long axis.

Repeated DSC scans at different heating/cooling rates (2, 5 and 10 °C/min) also could not detect the **N-N_{cybC}** transition with any noticeable transition enthalpy (**Figure4A.3.1.2**). At lower temperatures below this transition temperature (~135^{O}C) one could observe the diffuse small angle scattering maxima besides the meridian (dumb bell shape as shown in **Figures 4A.3.2.10c** at 132^{O}C, **10d** at 130^{O}C, **10e** at 127^{O}C) and the 2θ scans over the small angle diffraction gave the maxima at d = 41.4 Å (**Figure4A.3.2.11**) which is smaller than the molecular length of 42.1Å. The χ scans over the small angle region clearly indicated four symmetrically located diffuse maxima (**Figure4A.3.2.12a-c**, (tilt angle ~10.5^{o}) which confirmed this phase to be a cybotactic nematic phase with SmC type clusters.

Below 125.3^{O}C, we observed the growth of a striped pattern in the texture (phase-2) in cells treated for homogeneous (**Figure4A.3.2.7c**) and homeotropic alignments (**Figure4A.3.1.5 i, ii, iii and iv**). The growth of stripe pattern which is stable for 1.8^{o}C is accompanied by Brownian motion. Also this transition is not detected with any measurable enthalpy change in DSC study.

In the XRD pattern of the magnetically aligned sample, we observed two distinct types of diffuse small angle scattering maxima a) dumb-bell shaped maxima besides the meridian (tilted molecular arrangement) and b) maxima centred on the meridian (orthogonal molecular arrangement) (**Figure4A.3.2.10f**). The χ scan in the small angle region clearly indicated the two types of pattern viz., tilted and orthogonal molecular arrangement in nematic phase as shown in **Figure4A.3.2.12d**. The χ-scan at 125^{o}C (**Figure4A.3.2.16**) in the small angle region indicated by three peaks (blue line) indicate cybotactic SmA type cluster when compared to the two line pattern (red line) at 130°C indicative of cybotactic SmC type cluster. The intensity profile of 2θ scans (**Figure. 4A.3.2.17a**) gave maxima at d = 41.4Å and 41.9Å corresponding to **N_{cybC}** and **Nc_{ybA}** respectively and confirm the appearance of two types of coexisting molecular alignments of **N_{cybC}** and **Nc_{ybA}** in nematic phase. The width of the nematic phase possessing coexisting orthogonal and tilted cybotactic molecular alignments is found to be ~0.5^{o}C in X-ray studies while it is larger (~1.8^{o}C) in POM studies.

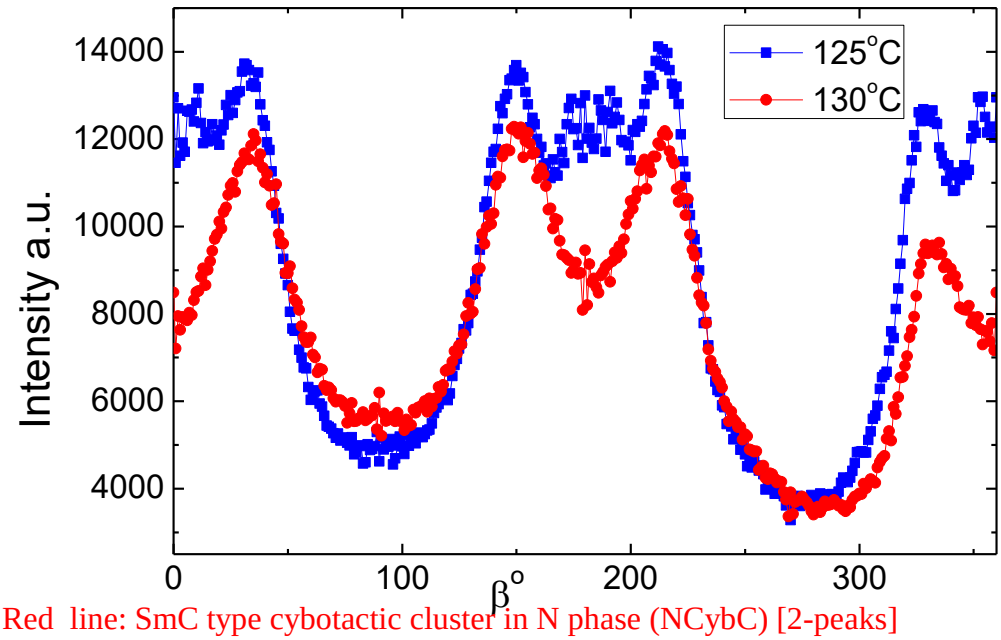

Figure 4A.3.2.16: Comparison of χ-scans over the small angle regions for **12-10** at temperatures 130^0C and 125^0C indicating the presence of coexistence of SmA and SmC cybotactic cluster in the nematic phase.

Further the variation in d-values (2θ scan from SAXS patterns, **Figure4A.3.2 17b**) and azimuthal angle (χ-scan, **Figure4A.3.2 17c**) with temperature confirmed the absence of any noticeable changes in cybotactic clustering of molecular alignment in nematic phase.

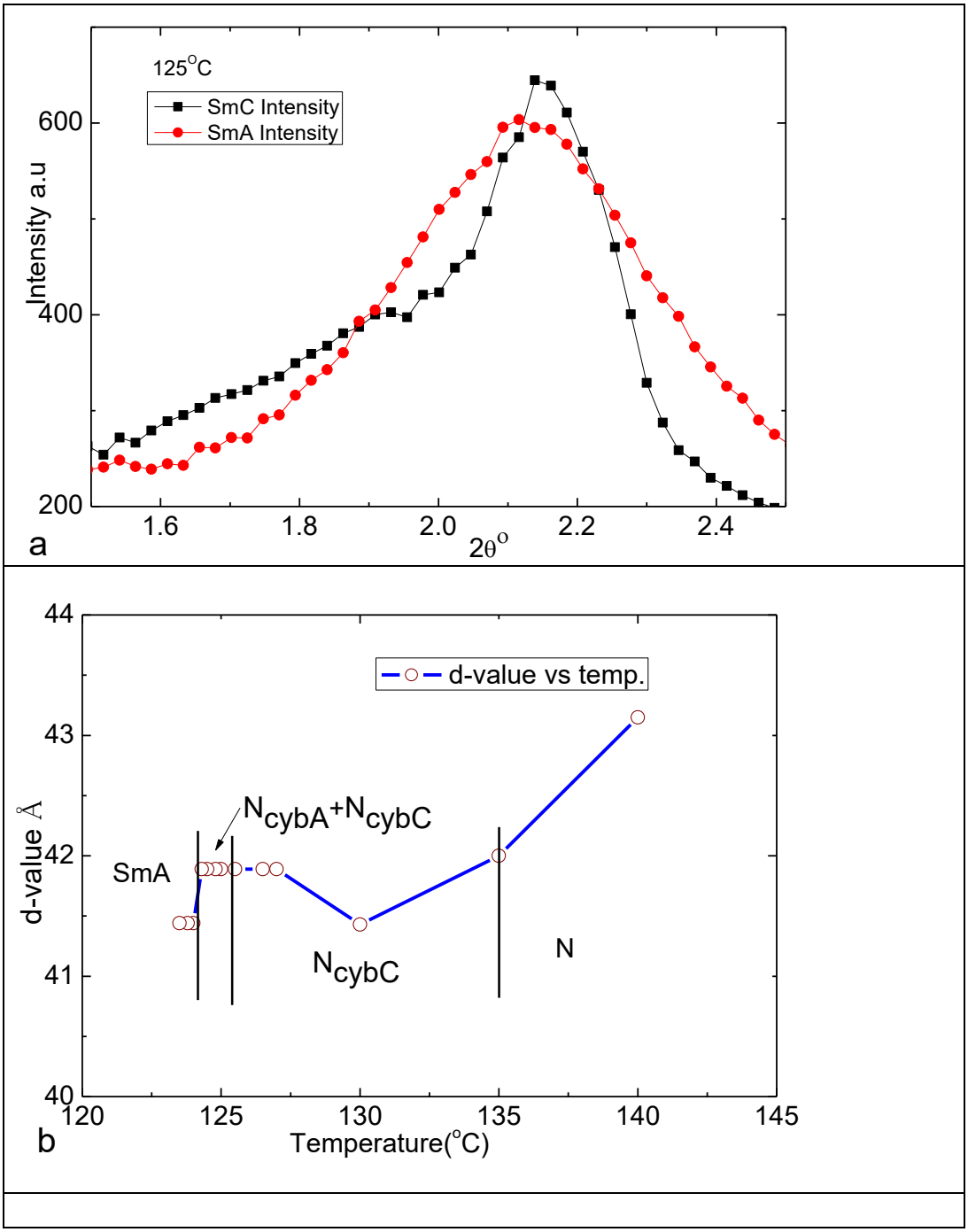
125°C
SmC Intensity
SmA Intensity
Intensity a.u
600
400
200
1.6
1.8
2.0
2.2
2.4
2θ°
a
d-value vs temp.
d-value Å
44
43
42
41
40
120
125
130
135
140
145
Temperature(°C)
SmA
N_cybA+N_cybC
N_cybC
N
b

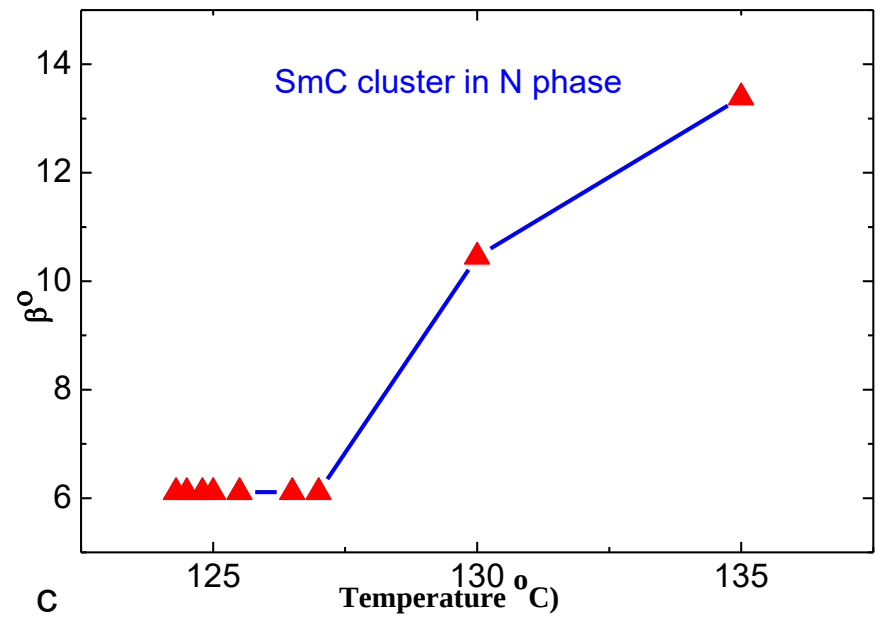

Figure4A.3.2.17: (a) Intensity profile of 2θ-scan in SAXS in the coexistence region (125^{0}C), (b) temperature dependence of d-values from SAXS and (c) temperature dependence of azimuthal angle (χ-values) from SAXS.

On further cooling phase-2 transformed into another mesomorphic phase (phase-3) by a very slow growth of two types of fan-like textures of opposite twist, which later transformed into cluster like regions with complimentary colours in adjacent domains and with a strong increase in birefringence as shown in **Figure4A.3.2. 8a-c**. In the XRD study, no changes appeared in the position and shape of the diffuse wide angle scattering (not shown here).

On reducing the temperature into phase-3 the position, shape and intensity of the wide angle scattering do not change, with a maximum at d = 4.96 Å corresponding to the mean lateral distance between the molecules, confirming the retention of fluidity of the liquid crystalline phase. However the SAXS pattern transformed into sharp Bragg peak (**Figure4A.3.2.10g**) with maxima at the meridian and has its maximum at d = 41.4 Å comparable with the molecular length L = 42.1 Å. This is consistent with a transition to a SmA phase indicating the orthogonal molecular alignment of the director. On further cooling the sample below 95°C transformed into a crystalline phase with sharp peaks at wide and small angle diffraction scatterings.

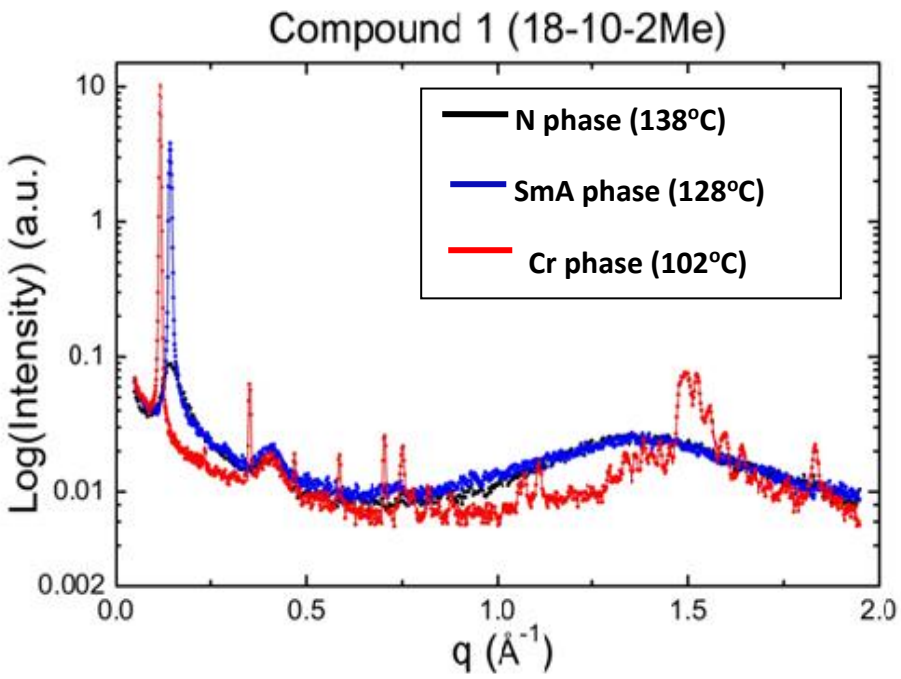

Figure4A.3.2.18(a): Intensity profile of q-scan at nematic, Smectic and crystalline temperature of **18-10**.

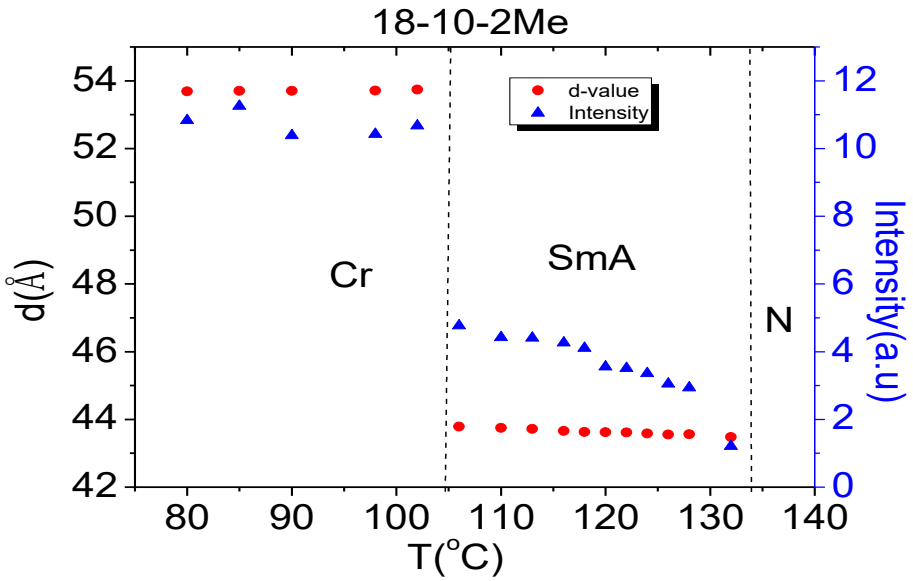

Figure 4A.3.2.18(b): Temperature dependence of d-values and intensity of **18-10.**

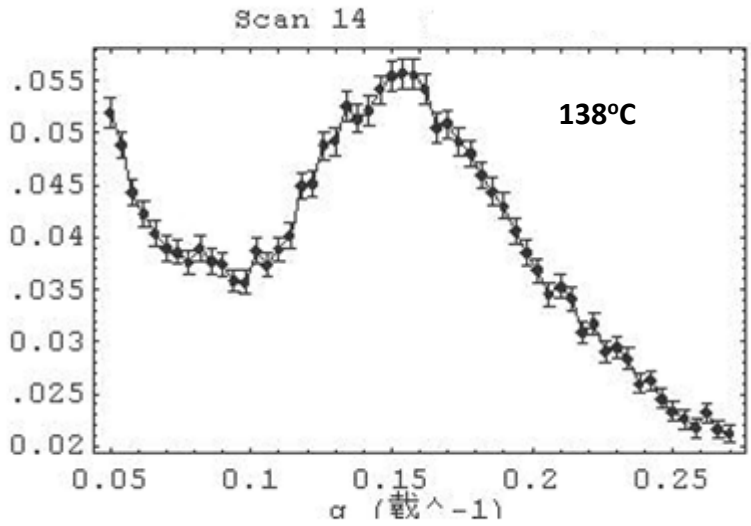

(a) Small angle intensity profile in nematic phase at T=138°C.

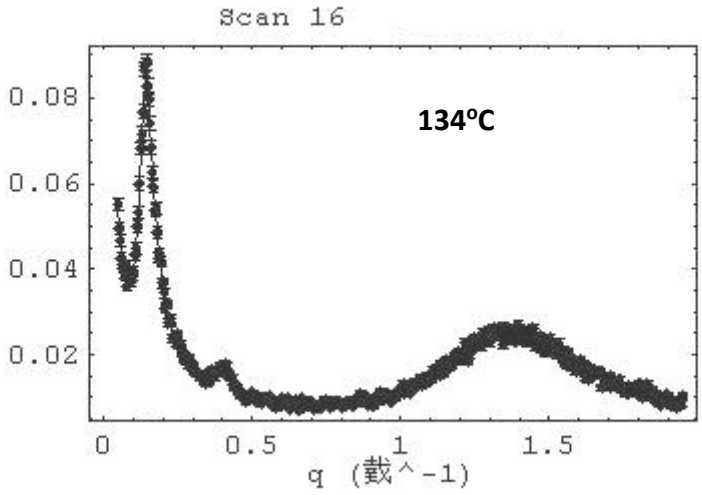

(b) Wide and small angle intensity profile in nematic phase at T=134°C.

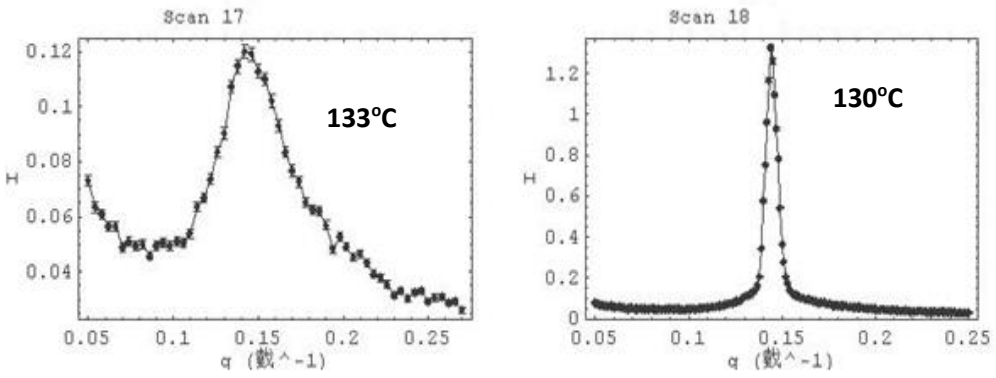

(c) Small angle intensity profile in nematic phase at T=133°C.

(d) Small angle intensity profile in smectic phase at T=130°C.

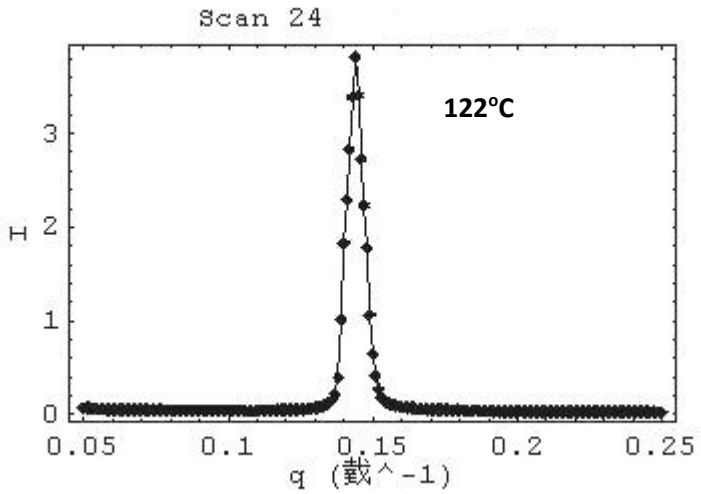

(e) Small angle intensity profile in smectic phase at T=122°C.

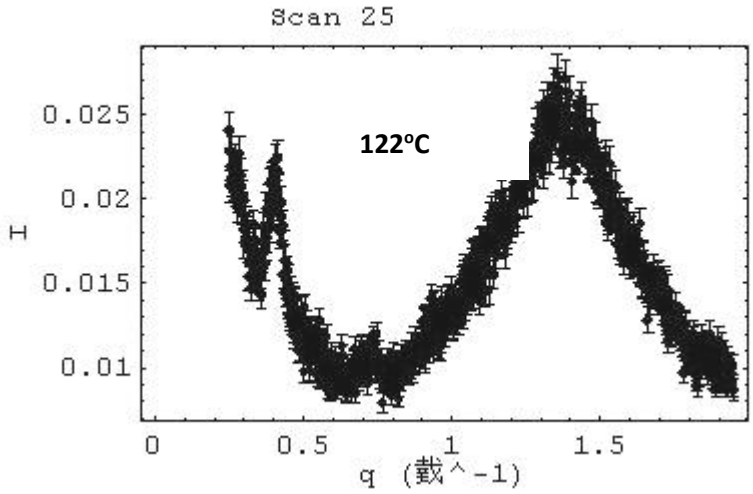

(f) Wide angle intensity profile in smectic phase at T=122°C.

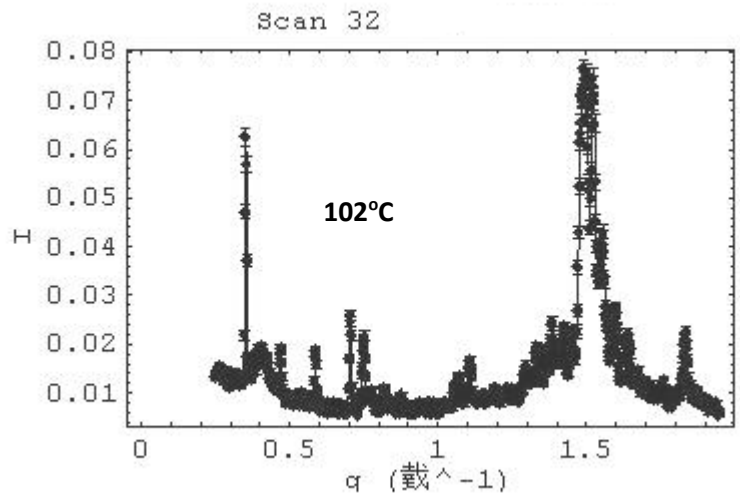

(g) Wide and small angle intensity profile in crystalline phase at T=102°C.

Figure 4A.3.2.19: Various intensity vs q^{-1} profile showing the nematic phase, SmA phase and crystalline phase in SAXS and WAXS.

Temperature variation of 2θ scan as a function of intensity in small angle region of **18-10** confirms different molecular arrangements in lower and higher temperature regions. The intensity of the SAXS is significantly higher than that of the diffuse wide angle scattering (**Figure4A.3.2.18a**). In the XRD study at T=138^{O}C (phase-1), the intensity profile as shown in **Figure 4A.3.2.18a** are centered on the equator indicating a fluid nematic phase. Cooling down to 128°C,

the intensity at small angle region changes from 0.1 to ~5 indicating orthogonal molecular arrangement; the signature of which is also found in DSC scan. It corresponds to the mean lateral distance between the molecules, confirming the retention of fluidity of the liquid crystalline phase. However the SAXS pattern transformed into sharp Bragg peak with maxima at the meridian and has its maximum at d = 43.9 Å comparable with the molecular length L = 44 Å; as evidenced from the energetically optimised preferred molecular structure shown in **Figure. 4A.3.2.13** in gaseous phase which was obtained from density functional theory studies at the B3LYP/6-31G(d) level basis set performed using ground state restricted *ab initio* Hartree-Fock calculations. On further cooling the sample at 102°C transformed into a crystalline phase with sharp peaks at wide and small angle diffraction scatterings.

4A.3.3 Absorption and Emission characteristics:

The UV absorption and fluorescence spectroscopic properties of compound 12-10 in solution were studied in various solvents of different concentrations to obtain information regarding absorption and emission maxima, and the Stokes shift of fluorescence. The compounds exhibited similar absorptions with absorption peaks at 353 nm (3.51 eV for toluene, ε ~100000 $Lmol^{-1}cm^{-1}$), 351 nm (3.53 eV for dichloromethane, ε ~ 189000 $Lmol^{-1}cm^{-1}$), 341 nm (3.63 eV for benzene, ε ~ 59000 $Lmol^{-1}cm^{-1}$) as depicted in **Figure 4A.3.3.20**. These absorption band with large molar absorption coefficients reflects the π-π* transition of the highly π-conjugated system having the substituted phenyl benzoate unit as the core.

The UV-visible spectra of 12-10 have been simulated using the time dependent density functional theory (TD-DFT) Becke3-Lee-Yang-Parr hybrid functional-6-31G (d, p) method. The experimental and theoretical absorbance as a function of wavelength is plotted in **Figure 4A.3.3.21**. The 3-D iso-surface plots of the highest occupied molecular orbital (HOMO) and lowest unoccupied molecular orbital (LUMO) of the complex are shown (F**igures 4A.3.3.22**). The HOMO and LUMO energies are calculated to be -5.57eV and -1.94 eV, respectively, ΔE= 3.63 eV. The HOMO–LUMO energy separation can be used as a measure of

kinetic stability of the molecule and could indicate the reactivity pattern [29,30]. A large HOMO–LUMO gap implies a high-kinetic stability and low chemical reactivity, because it is energetically unfavourable to add electrons to a high lying LUMO or to extract electrons from a low-lying HOMO [30]. The HOMO–LUMO energy gap of 3.63 eV suggests that the compound is fairly stable.

Additionally, we investigated the fluorescence spectrum to observe the characteristic features of the excited states of 12-10 as shown in **Figure 4A.3.3.23**.

The fluorescence emission spectra of these compounds were examined in chloroform solution (conc. 10^{-3}, 10^{-4} and 10^{-5} M) and it was found that all exhibited strong fluorescence on excitation at 350 nm. The emission peak at λ_{em} = 510 nm (2.43 eV) for compound 12-10, with a large Stokes shift λ_S of the order of λ_S = 160 nm was attributed to the formation of intermolecular excimers. This Stokes shift, which reflects the structural relaxation of the excited molecule, is significantly larger than in reported push-pull systems exhibiting liquid crystal behaviour,[31] indicating that the molecular conformation changes upon excitation. The plots of the fluorescence spectra at different excitation wavelengths show that the relative intensity of the peak at 510 nm gradually increases with increasing excitation wavelength.

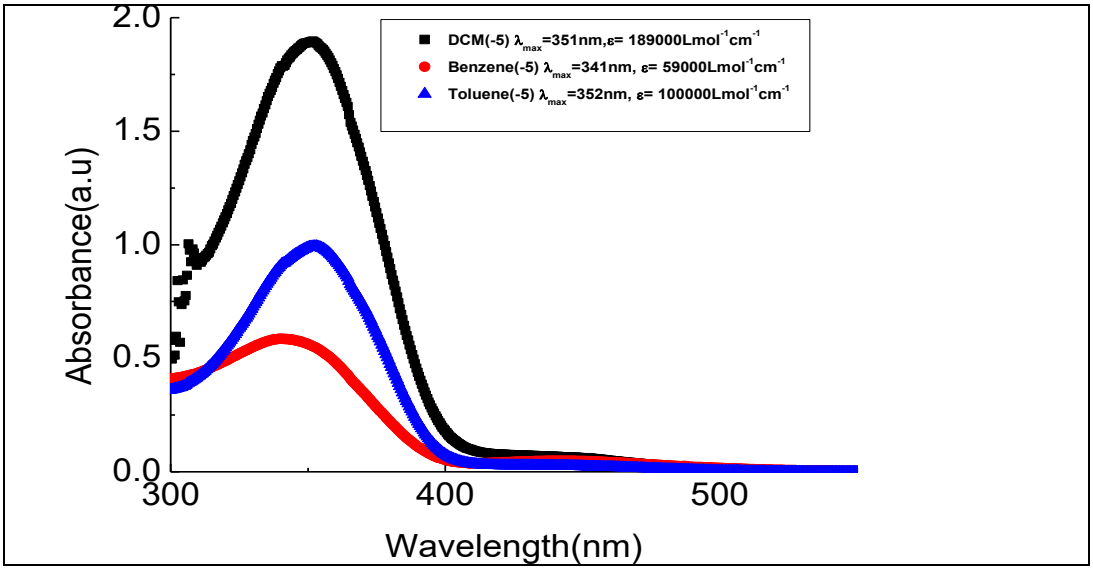

Figure 4A.3.3.20: UV-Visible spectra of 12-10**.**

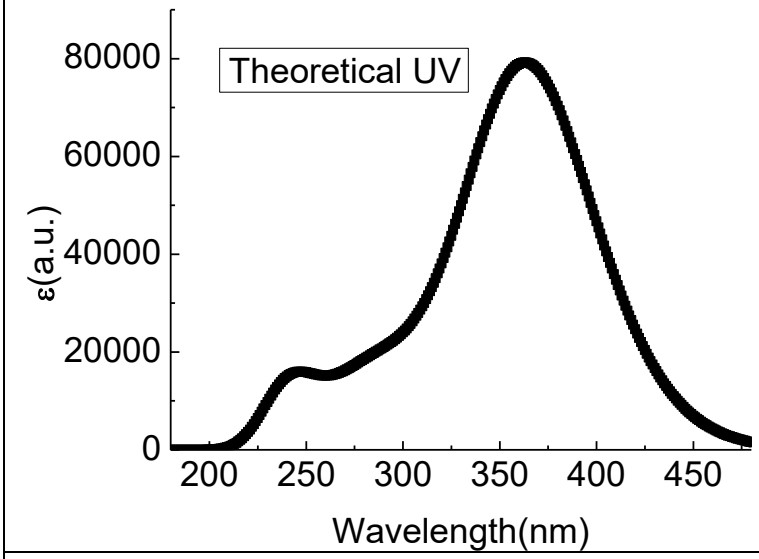

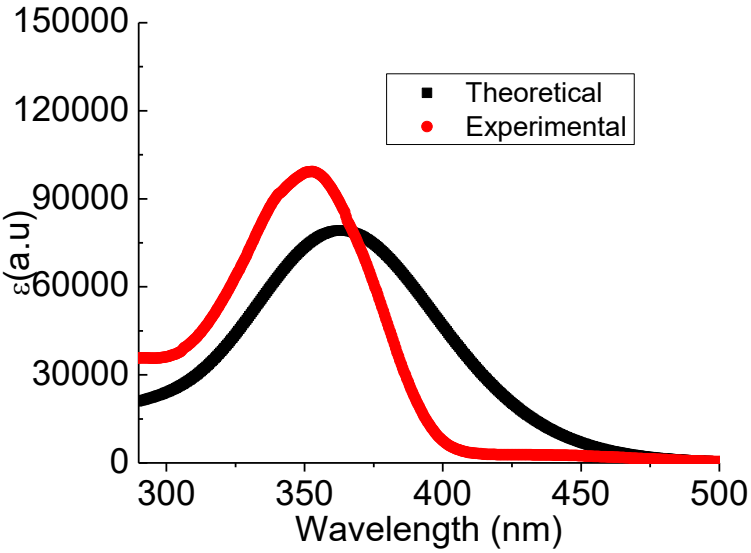

Figure 4A.3.3.21: Theoretical and experimental UV spectra of 12-10.

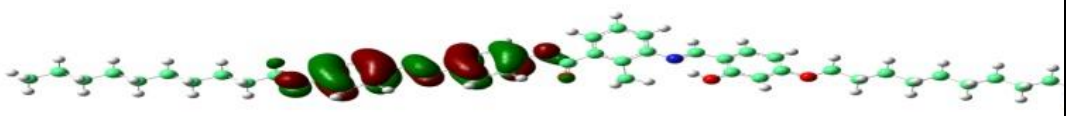

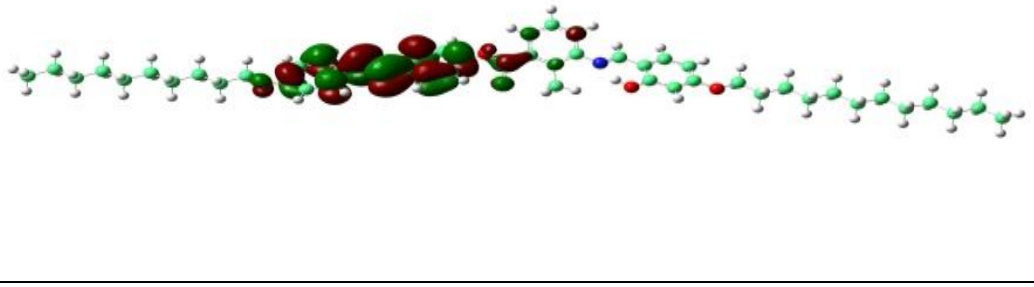

Figure 4A.3.3.22: HOMO and LUMO of 12-10.

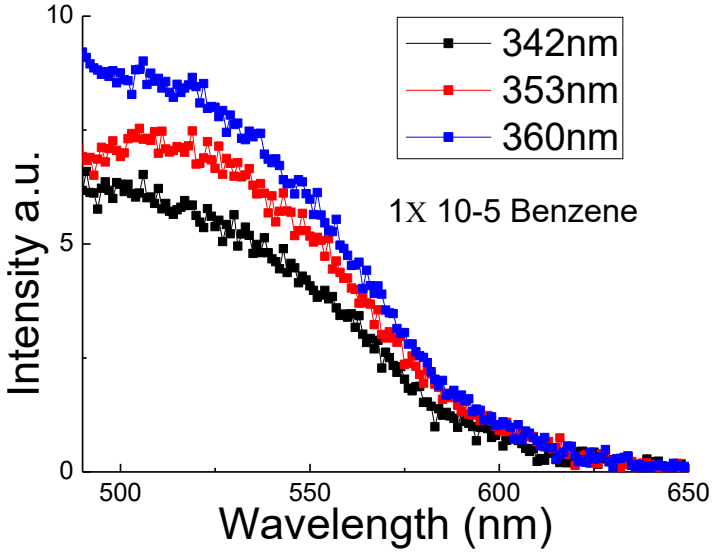

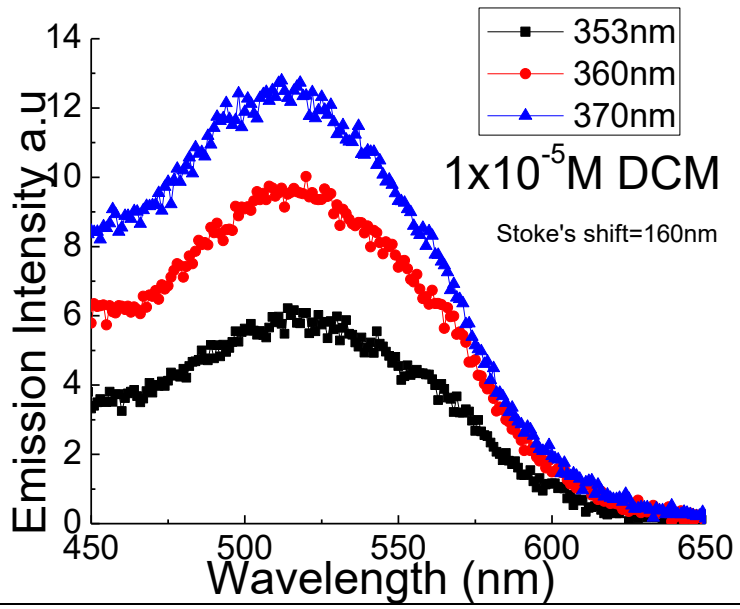

Figure 4A.3.3.23: Fluorescence spectra of 12-10 in benzene at various excitation wavelengths.

4A.4. Conclusion:

Majority of the four-ring bent core compounds reported so far in literature [32-36] do not exhibit banana mesomorphism. However in some compounds [36] SmA, SmC and SmI phases can be transformed into polar structures under the influence of electric field. In another four-ring compound derived from oxadiazole [7f] exhibits a nematic, a SmC and optically isotropic phase (chiral Bx) with randomly distributed domains of opposite handedness. Classical Four-ring system derived from 1,3-phenylene moiety[34c] substituted with three fluoro substituents exhibited chiral SmA* and SmC* phases while the unsubstituted compound do not show mesomorphism. It is remarkable that the exhibition of banana mesomorphism in an earlier communication and nematic and smectic phase with distinctly different molecular orientation presented in this work respectively, by the classical four-ring bent-core system with modifications of bridging groups or substituents, demonstrated the importance of these materials and is therefore of high priority. The importance of substituents, influence of bridging groups, steric and van der Waals interactions etc have origins in basic structure–property relationships and the observed smectic mesophases and polar structures in these materials research opened lot of intriguing questions which requires further systematic investigations. Experimental examples of orientationally ordered but spatially homogeneous liquid phases are rare among the bent-core molecules. In conclusion the four-ring bent core systems are able to form traditional polar banana phases[26] as well as nematic phase with classical molecular alignment of calamitic type as well as cybotactic nematic *SmC* type, coexisting $N_{\mathbf{cybC}}$ and $N_{\mathbf{cybA}}$ phase and *SmA* phases in the present work, depending on the nature and position of substituents, linking group and its direction. X-ray and different other experimental studies confirm the phase sequence as N-NcybC-coexisting $N_{\mathbf{cybC}}$-$N_{\mathbf{cybA}}$ -SmA-Cr in the four-ring bent core system of hockey stick shaped molecules under investigation. Hence the four-ring bent core systems are of great importance as their study form the boundary between calamitic and banana shaped compounds of five- and six- ring compounds.

References:

[1] T. Niori, T. Sekine, J. Watanabe, T. Furukawa and H. Takezoe, *J. Mater. Chem.*, **6**, 1231-1233,(1996).

[2] D. R. Link, G. Natale, R. F. Shao, J. E. Maclennan, N. A. Clark, E. Korblova and D. M. Walba, *Science*, **278**, 1924-1927, (1997).

[3] (a) H. Takezoe and Y. Takanishi, *Jpn. J. Appl. Phys.*,**45**, 597-625, (2006); (b) R. A. Reddy and C. Tschierske, *J. Mater. Chem.*, **16**, 907–961, (2006); (c) M. B. Ros, J. L. Serrano, M. R. de la Fuente and C. L. Folcia, *J. Mater. Chem.*, **15**, 5093-5098, (2005); (d) C. Tschierske and G. Dantlgraber, *Pramana*, **61**, 455-481, (2003); (e) G. Pelzl, S. Diele and W. Weissflog, *Adv. Mater*., **11**, 707–724, (1999).

[4] D. A. Coleman, J. Fernsler, N. Chattham, M. Nakata, Y. Takanishi, E. Korblova, D. R. Link, R. F. Shao, W. G. Jang, J. E. Maclennan, O. M. Monval, C. Boyer, W. Weissflog, G. Pelzl, L. C. Chien, D. M. Walba, J. Zasadzinski, J. Watanabe, H. Takezoe and N. A. Clark, Science, **301**, 1204–1211, (2003).

[5] (a) C. Tschierske and D. J. Photinos, *J. Mater. Chem.*, **20**,4263-4294, (2010); (b) M. Lehman, *Liq. Cryst. Today*, **18**, 31-34, (2009); (c) V. Gortz, *Liq. Cryst. Today*, **19**, 37-48, (2010).

[6] (a) V. Prasad, S. W. Kang, K. A. Suresh, L. Joshi, Q. Wang and S. Kumar, *J. Am. Chem. Soc.*, **127**, 17224-17228, (2005); (b) K. Van Le, M. Mathews, M. Chambers, J. Harden, Q. Li, H. Takezoe, and A. Jakli, *Phys. Rev. E: Stat., Nonlinear, Soft Matter Phys.,* **79**, 030701, (2009); (c) H. G. Yoon, S. W. Kang, R. Y. Dong, A. Marini, K. A. Suresh, M. S.Rao and S. Kumar, *Phys. Rev. E: Stat., Nonlinear, Soft Matter Phys.*, **81**, 051706, (2010); (d) G. Pelzl, A. Eremin, S. Diele, H. Kresse, W. Weissflog, *J. Mater. Chem.*, ***12***, 2591-2593, (2002); (e) T. Niori, J. Yamamoto, H. Yokoyama, *Mol. Cryst. Liq. Cryst*., **409**, 475-482, (2004); (f) W. Weissflog, S. Sokolowski, H. Dehne, B. Das, S. Grande, M. W. Schröder, A. Eremin, S. Diele, G. Pelzl, H. Kresse, *Liq. Cryst.,* **31**, 923-933, (2004); (g) M. Hird, Y. Raoul, J. W. Goodby, H. F. Gleeson, *Ferroelectrics, **309***, 95-101, (2004); (h) C. Keith, A. Lehmann, U. Baumeister, M. Prehm and C. Tschierske, *Soft Matter*, **6**,1704-1721, (2010).

[7] (a) L. A. Madsen, T. J. Dingemans, M. Nakata and E. T. Samulski, *Phys. Rev. Lett.*, **92**, 145505, (2004); (b) T. J. Dingemanns, L. A. Madsen, N. A. Zafiropoulos, W. Lin and E. T. Samulski, *Philos. Trans. R. Soc. London, Ser. A*, **364**, 2681-2696, (2006); (c) N. A. Zafiropoulos, W. Lin, E. T. Samulskii, T. J. Dingemans and S. J. Picken, *Liq. Cryst.*, **36,** 649-656, (2009); (d) V. Gortz and J. W. Goodby, *Chem. Commun.*, 3262-3264, (2005); (e) V. Gortz, C. Southern, N. W. Roberts, H. F. Gleeson and J. W. Goodby, *Soft Matter*, **5**, 463-471, (2009); (f) S. Kang, Y. Saito, N. Watanabe, M. Tokita, Y. Takanishi, H. Takezoe and J. Watanabe, *J. Phys. Chem. B*, **110**, 5205-5214, (2006).

[8] M. W. Schroder, S. Diele, G. Pelzl, U. Dunemann, H. Kresse and W. Weissflog, *J. Mater. Chem.*, **13**, 1877-1882, (2003).

[9] (a) R. Stannarius, A. Eremin, M. G. Tamba, G. Pelzl and W. Weissflog, *Phys. Rev. E: Stat., Nonlinear, Soft Matter Phys.*, **76**, 061704, (2007); (b) C. V. Yelamaggad, S. Shashikala, D. S. Shankar Rao, C. V. Lobo and S. Chandrasekhar, *Angew. Chem., Int. Ed.*, **43**, 3429-3432, (2004).

[10] (a) M. Lehmann, C. Kohn, H. Kresse and Z. Vakhovskaya, *Chem. Commun.*, 1768-1770, (2008); (b) M. Lehmann, C. Kohn, J. L. Figueirinhas, G. Feio, C. Cruz and R. Y. Dong, *Chem. Eur J.* ,**16**, 8275-8279, (2010); (c) M. Lehmann, S. W. Kang, Ch. Kohn, S. Haseloh, U. Kolb, D. Schollmeyer, Q. Wang and S. Kumar, *J. Mater. Chem.*, **16**, 4326-4334, (2006); (d) M. Lehmann and J. Levin, *Mol. Cryst. Liq. Cryst.*, **411**, 273-281, (2004).

[11] G. R. Luckhurst Nature , **430**,413-414, (2004).

[12] M. J. Freiser, *Phys. Rev. Leu.*, **24**, 1041-1043, (1970).

[13] G. R. Luckhurst, *Thin Solid Films*, **393**, 40-52, (2001).

[14] K. Praefcke, *Mol. Cryst. Liq. Cryst.*, **364**, 15, (2001).

[15] G. R. Luckhurst, *Angew. Chem., Int. Ed.*, **44**, 2834-2836, (2005).

[16] D. W. Bruce, *Chem. Rec.*, **4**, 10, (2004).

[17] E. T. Samulski., Liq. Cryst., **37**, 669-678, (2010).

[18] S. Chandrasekhar, G. G. Nair, D. S. S. Rao, S. K. Prasad, K. Praefcke, D. Blunk,. *Liq. Cryst. ,**24***, 67–70, (1998).

[19] (a) B. R. Acharya, A. Primak, and S. Kumar, Phy Rev. Lett. ,**92**, 1455506, (2004); (b) B. R. Acharya, S. W. Kang and S. Kumar, Liq. Cryst., **35**, 109,

(2008); (c) B. R. Acharya, S. W. Kang, V. Prasad and S. Kumar, J. Phys. Chem. B, **113**, 3845, (2009).

[20] A. Gudkov, J. Struct. Chem, **33**, 436-442, (1992) .

[21] A. de Vries, Mol. Cryst. Liq. Cryst. ,**10**¸ 219-236, (1970).

[22] O. Francescangeli, V. Stanic, S. I. Torgova, A. Strigazzi, N. Scaramuzza, C. Ferrero, I. P. Dolbnya, T. M. Weiss, R. Berardi, L. Muccioli, S. Orlandi, and C. Zannoni, Adv. Funct. Mater. **19**, 2592-2600, (2009).

[23] O. Francescangeli, and E. T. Samulski, Soft Matter , **6**, 2413-2420, (2010).

[24] O. Francescangeli,, F. Vita, C. Ferrero, T. J. Dingemans and E. T. Samulski, Soft Mater,**7**, 895-901, (2011).

[25] S. J. Pikin, T. J. Dingemans, L. A. Madsen, O. Francescangeli and E. T. Samulski., Liq. Cryst., **39**,19-23, (2012)

[26] (a) R. Deb, R. K. Nath, M. K. Paul, N. V. S. Rao, F. Tuluri, Y. Shen, R. Shao, D. Chen, C. Zhu, I. I. Smalyukh and N. A. Clark, *J. Mater. Chem.*,**20**, 7332-7336, (2010); (b) D. K. Yoon, R. Deb, D. Chen, E. Korblova, R. Shao, K. Ishikawa, N. V. S. Rao, D. M. Walba, I. I. Smalyukh and N. A. Clark, *Proc. Nat. Acad. Sci.*, **107**, 21311-21315, (2010).

[27] (a) D. Shen, S. Diele, I. Wirth and C. Tschierske, *Chem. Commun.*, 2573-2574, (1998); (b) D. Shen, A. Pegenau, S. Diele, I. Wirth and C. Tschierske, *J. Am. Chem. Soc.*, **122**, 1593-1601, (2000).

[28] (a) C. Prasang, A. C. Whitwood and D. Bruce, *Chem. Commun.*, 2137-2139, (2008); (b) P. S. Salter, P. W. Benzie, R. A. Reddy, C. Tschierske, S. J. Elston, and E. P. Raynes, *Phys Rev E, : Stat., Nonlinear, Soft Matter Phys.,* **80**, 031701, (2009).

[29] K.H. Kim, Y.K. Han, J. Jung. Theor. Chem. Acc., **113**, 233 (2005).

[30] J. Aihara. J. Phys. Chem. A, **103**, 7487 (1999).

[31] C. V. Yelamaggad, I. S. Shashikala, U. S. Hiremath, G. Liao, A. Jakli, D. S. S.Rao, S. K. Prasad, Q. Li, *Soft Matter*, **2**, 785, (2006).

[32] F. C. Yu and L. J. Yu, *Chem Mater*., **18**, 5410-5420, (2006).

[33] T. Masuda and Y. Matsunaga, *Bull. Chem. Soc. Jpn*., **64**, 2192-2195, (1991).

[34] (a) M. Hird, J.W. Goodby, N. Gough, K.J. Toyne, *J. Mater. Chem.*,**11**, 2732-2742, (2001)., (b) K. M. Fergusson and M. Hird *Adv.Mater*., **19**, 21-214, (2007),(c) K. M. Fergusson and M. Hird , *J.Mater. Chem*., **20**, 3069-3078, (2010).

[35] J. H. Wild, K. Bartle, M. O'Neill, S. M. Kelly and R. P. Tuffin, *Liq.Cryst*., **33**, 635-644, (2006).

[36] W. Weissflog , U. Dunemann, S. F. Tandel, M. G. Tamba, H. Kresse, G. Pelzl, S. Diele, U. Baumeister, A. Eremin, S. Stern and R. Stannarius, *Soft Mater*, **5**, 1840-1847, (2009).

Chapter IV

Results and Discussion

Part B

Study of stripe domains, Freedricksz transition and the elastic constants in the nematic phase.

4B.1.Introduction:

The discovery of polar and chiral smectic phases in achiral bent core liquid crystals [1-3] led to new activities in these materials with functional properties. The manifestation of nematic phases among the mesophases in materials of bent core molecules is relatively scarce due to strong tendency for smectic layering generated by the close packing of the kinked molecules promoted by aromatic core interactions [4]. Further the discovery of fluid cybotactic nematic phases [5-9] (formed by Sm-C like clusters viz., N_{cybC} phase) with ferroelectric response and field induced biaxiality in the nematic phase of bent-core mesogens derived from symmetrical 3,5-diphenyl-1,2,4-oxadiazole unit is reported [10]. The same phenomenon was corroborated in unsymmetrical 1,2,4-oxadiazole derivatives with a cyclohexene end moiety [11, 12]. The transition from normal to skewed cybotactic nematic phase exhibited by some bent-core nematic mesogens as evidenced by small angle X-ray studies [7] is correlated to N_U-N_B phase transition by optical textures [13]. However only recently asymmetric achiral four-ring bent-core compounds of N-benzoylpiperazine derivatives [14], low melting unsymmetrical four-ring bent-core 1,3-disubstituted phenylene derivatives [15], $4^{/}$-amino phenyl-3-aminobenzoate derivatives exhibiting smectic phases have been reported [16,17]. The investigations of structure-property relationship in these four ring bent core compounds are of specific interest because their molecular structure is at the boundary between banana-shaped five-ring and rod-like liquid crystals. The unusual physical properties reported [18-23] in mixtures of bent-core and rod-like compounds motivated us to study the physical properties like stripe patterns, elastic constants etc in nematic phases. The realization of nematic phases in achiral four-ring bent-core molecules is dependent on the molecular architecture with extended aromatic cores and/or relatively shorter terminal chains or reduction of molecular bent promoted by a substituent in the bent position. We succeeded in the realization of cybotactic nematic phase with smectic C type clusters (N_{cybC}) in four-ring bent-core compounds in addition to two more phases viz., Nx phase (with coexistence of N_{cybC} and cybotactic nematic phase with smectic A type clusters (N_{cybA})) and SmC phase. The molecular structure and transition temperatures of the compound **12-10** [24] are presented in

Figure 4B.1. To measure the elastic constants we prepared the binary mixtures of 5% and 7% of four-ring bent core molecule **12-10** with n-heptylcyanobiphenyl (7CB) exhibiting nematic phase. Here after these mixtures are abbreviated as 5M and 7M respectively. Both the mixtures 5M and 7M exhibited nematic phases with positive dielectric anisotropy and the transition temperatures are given below.

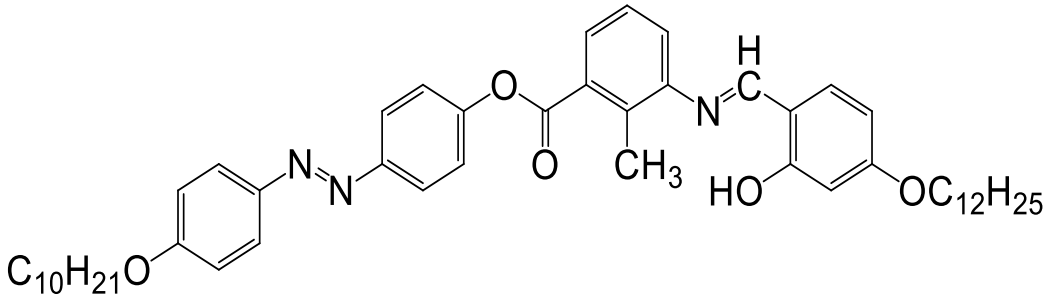

Figure 4B.1: Chemical structure of the compound 12-10**.**

12-10: Iso 148.9ºC N 135.0ºC N_{cybC} 125.3ºC Nx 123.5ºC SmC 92.9ºC Cr

N5: (5%N 1210 + 95% 7CB): Iso 48.3ºC N < 25.0 ºC Cr

N7: (7%N 1210 + 93% 7CB): Iso 53.3ºC N < 25.0 ºC Cr

4B.2.Results and Discussion:

The compound exhibits negative dielectric anisotropy and the homeotropic alignment of the same could not be achieved with different alignment agents like silane coupling, cytope, SE-1211 and JALS-204. **Figure 4B.2.2** shows the polarizing optical microscopic (POM) photographs of striped texture of **12-10** in a 5.0 μm thick cell treated with different homeotropic alignment materials in Nx phase (cybotactic nematic phase possessing two distinct molecular arrangements of N_{cybC} and N_{cybA}).

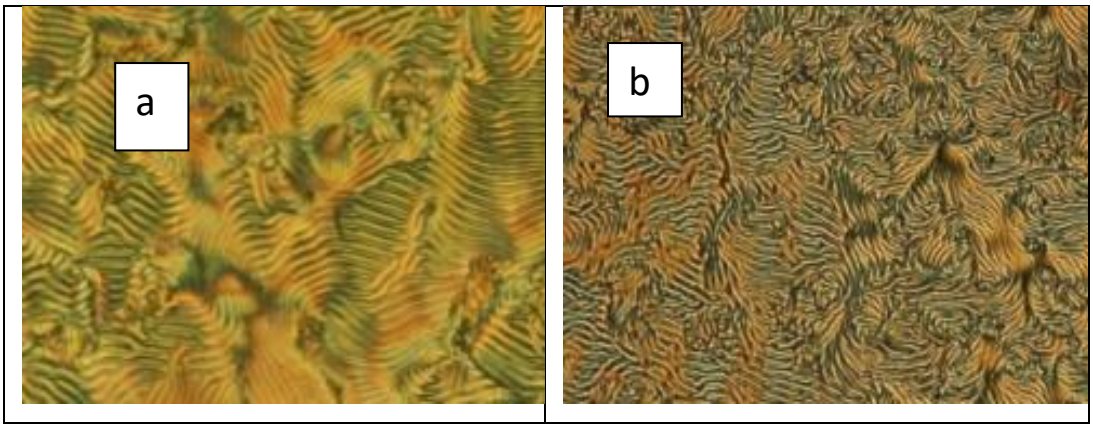

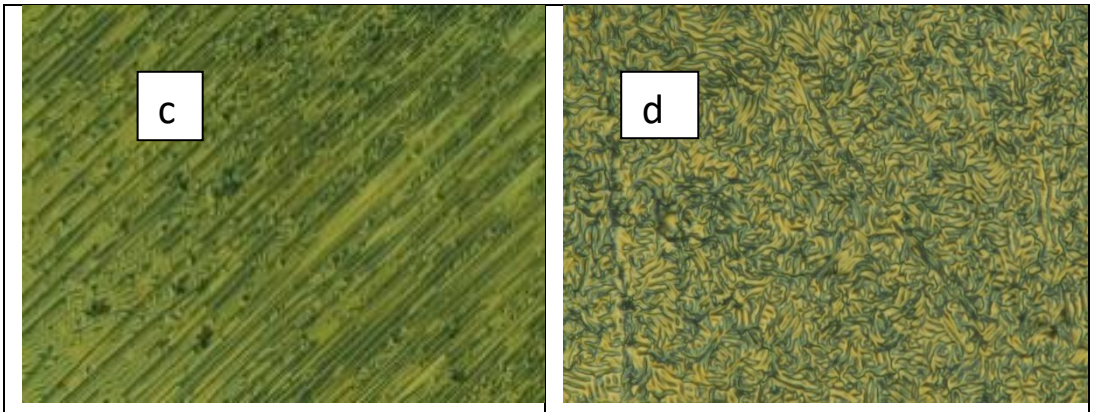

Figure 4B.2.2: Observed stripe pattern in homeotropically aligned cells treated with different alignment agents (a) Silane coupling (b) Cytope (c) SE-1211 (d) JALS-204, T = 125^{o}C.

The thermal range of the Nx phase is 1.8^{o}C and exists between cybotactic nematic phase and smectic A phase. The stripe patterns appeared on cooling and they gradually filled the entire area of the cell. Application of a small electric field (up to 5 V/µm) did not affect the observed striped pattern. The observed stripes are well defined with distinct optical contrast. Eight different cells with varying thickness 1.5 µm to 12.3 µm were prepared with Silane coupling agent as alignment layer and the periodicity was measured for stripes appearing near smectic transition. The measured stripe period (**D**) and square of stripe period ($\mathbf{D^2}$) variation as a function of cell thickness (**d**) is shown in **Figure 4B.2.3a. D** varied from 2.1µm to 5.3 µm in cells of different thickness. The stripe period is found to be temperature independent in the entire phase range. **Figure 4B.2.3b** shows the variation of $\mathbf{D}^2$ as function of **d** and the experimental data represents a straight line with $\mathbf{D}^2$ is proportional to **d**. The stripe pattern resembled the spontaneous periodic director modulation reported earlier [25, 26] and the reason for such stripe formation is ascribed due to the high splay-bend and twist-bend elastic anisotropy with rather weak anchoring energy [27].

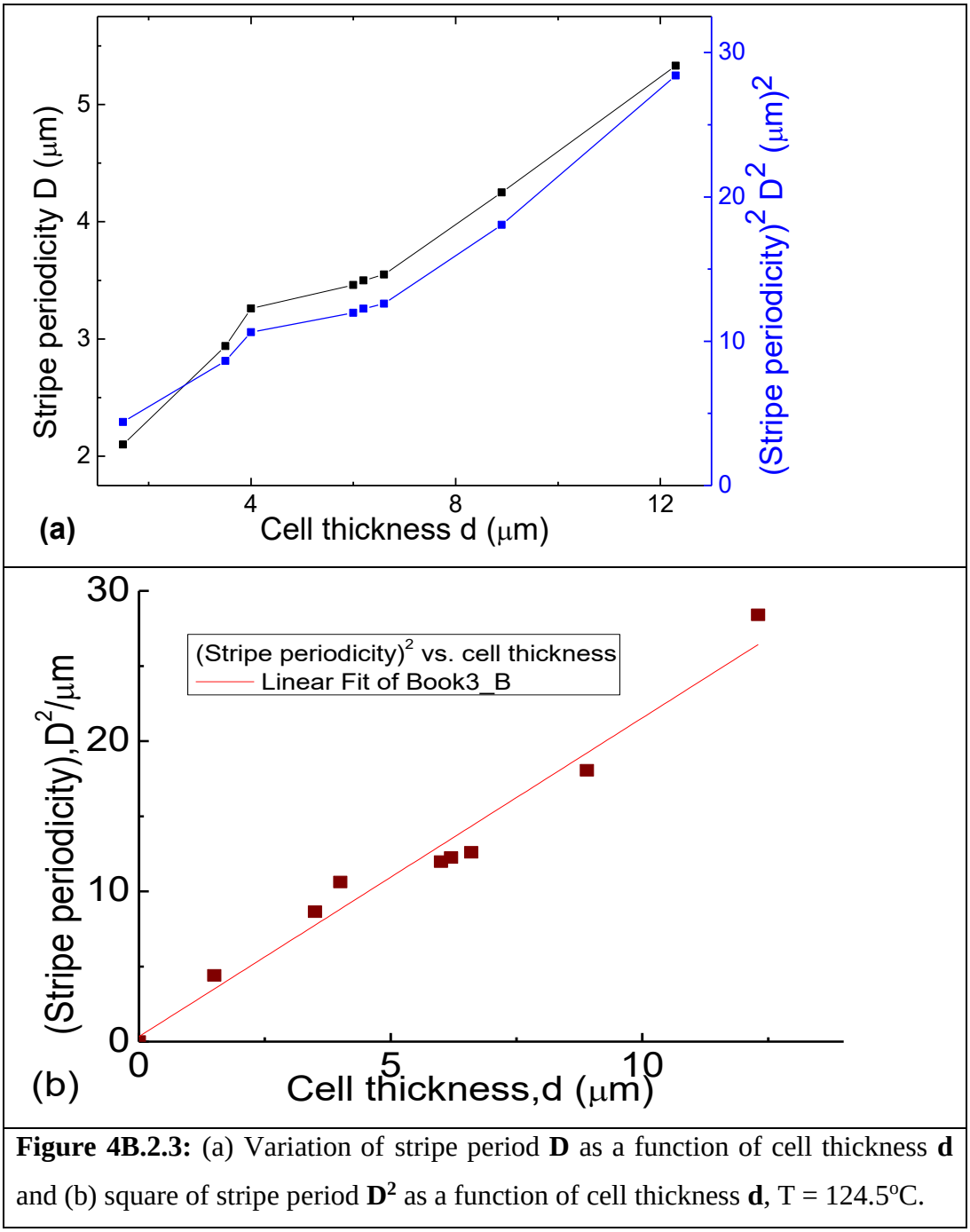

Figure 4B.2.3: (a) Variation of stripe period **D** as a function of cell thickness **d** and (b) square of stripe period $\mathbf{D^2}$ as a function of cell thickness **d**, T = 124.5^{o}C.

4B.3.Influence of UV-Visible light on the stripe formation in Nx phase:

The temperature range of the Nx phase, exhibiting the stripe pattern in a homeotropic cell, was found to be dependent on UV-Visible light. The temperature range of Nx phase with the stripe pattern remains for 1.8 ^{o}C before transition. Insertion of yellow filter which cuts the UV-Visible light below 460nm, the stripe pattern exists for only 0.8 ^{o}C above the SmA phase, which

further decreased to 0.3ºC upon insertion of orange filter (replacing the yellow filter) which cuts the light below 540nm. In presence of red filter the stripe pattern was observed as a transient phenomenon. The decrease in Nx phase temperature which decreased due to the exposure to UV-Visible light reflects the cis-trans photoisomerization (**Figure 4B.3.4)** of isomers and ca change in ratio of cis to trans isomers in the sample.

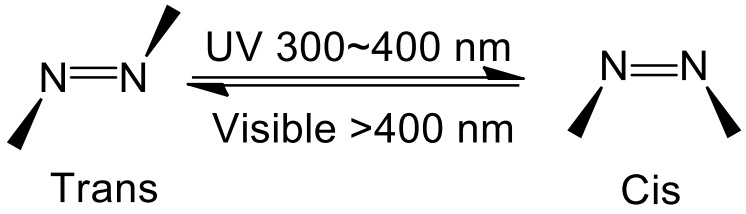

Figure 4B.3.4: Azobenzene photoisomerization, trans-form can be converted to cis-form using UV light (300 ~ 400 nm) and cis-form can be converted to trans-form by visible light.

It is also observed that the stripe pattern periodicity is dependent on the intensity ($\mu W/cm^2$) of UV-Visible light of the polarizing microscope as shown in **Figure 4B.3.5,** which increases linearly with the intensity. The cell used was treated for homeotropic alignment with a silane coupling agent and the cell thickness was 8.9μm.

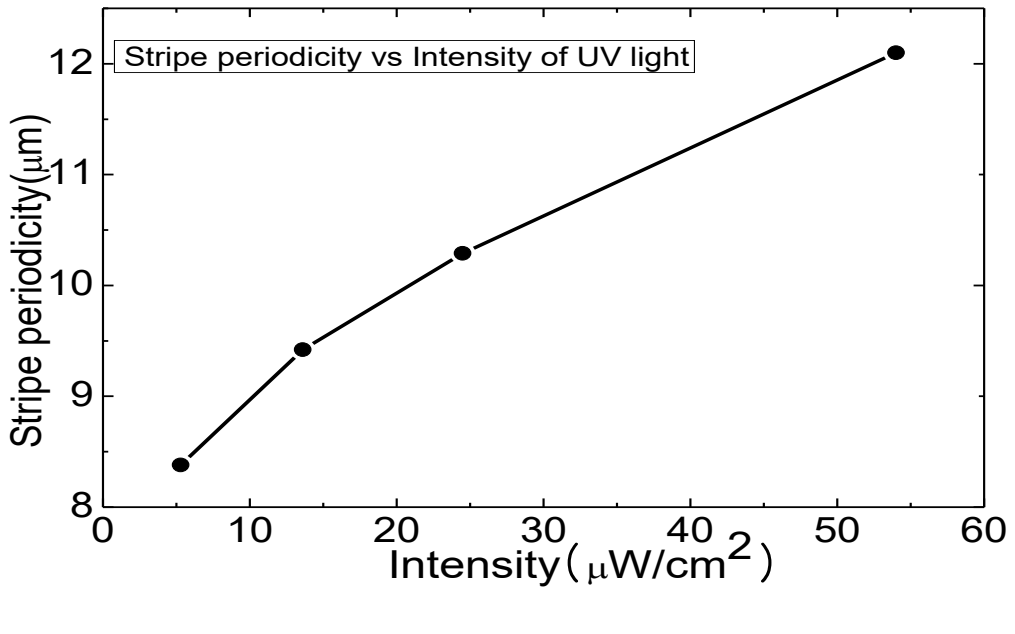

Figure 4B.3.5: Stripe pattern periodicity (**D**) variation as a function of Intensity of UV-Visible light, T =124.5ºC.

DFT optimized energy minimized molecular structure of **12-10** is shown in **Figure 4B.3.6a,** with a magnified image of molecular conformational structure with dipole-moment directed toward the bend or bow axis direction as shown in **Figure 4B.3.6b.** The resultant dipole-moment is 4.99 D. In the case of bent-core compounds with $\Delta\varepsilon < 0$, the dipole-moment (**μ**) component parallel to the bow axis, i.e. almost perpendicular to polarizability of the molecule (**P**) and both **μ** and P have similar alignment effects, i.e. planar alignment of the molecules **(Figure 4B.3.6d**). As a result, dielectrically-negative-type bent-core nematic compounds in general do not align homeotropic alignment.

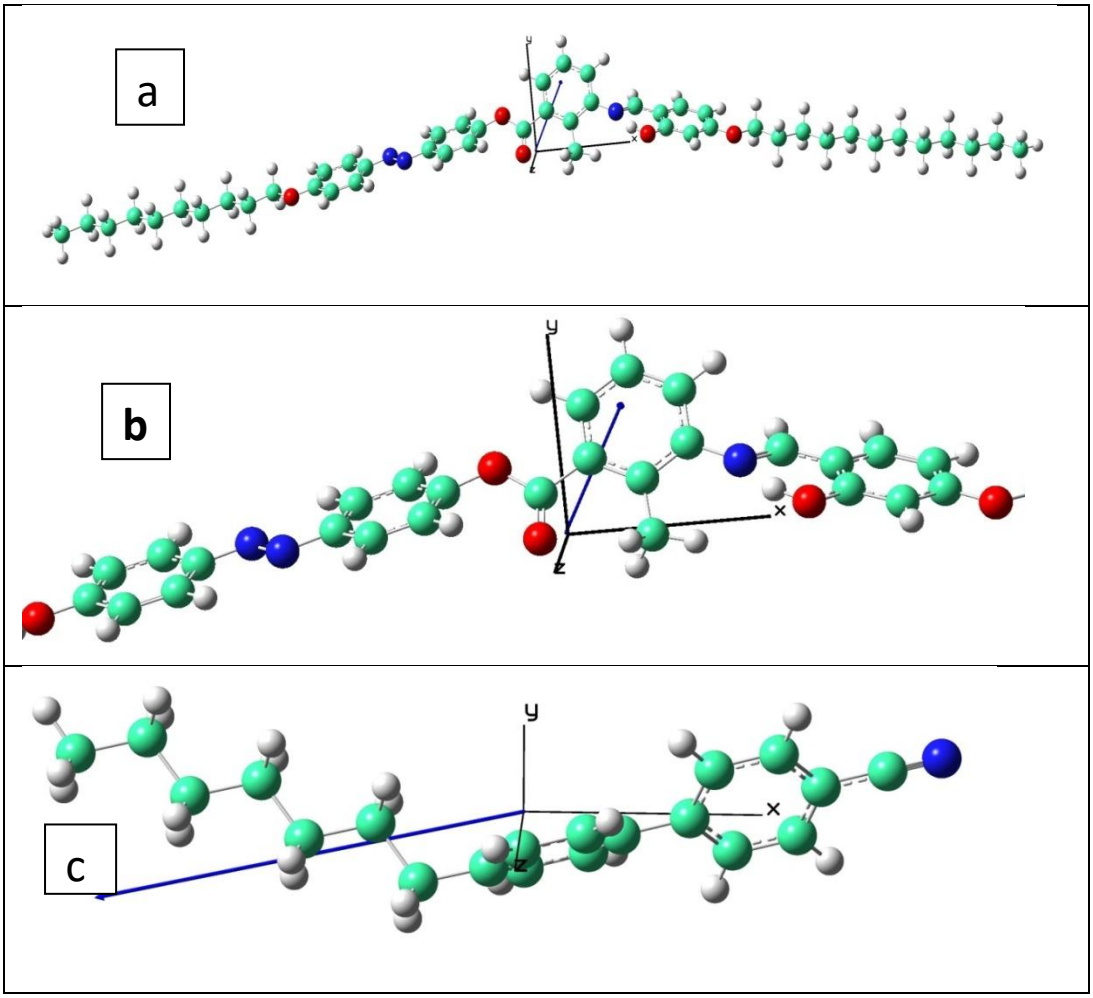

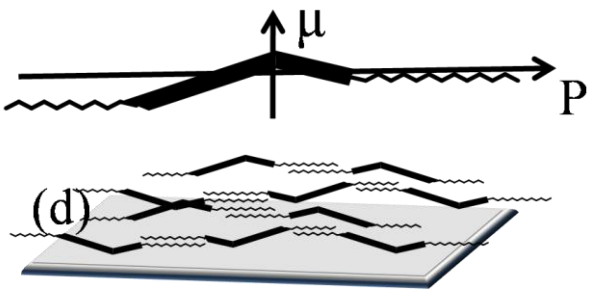

Compounds	μ_X	μ_Y	μ_Z	$\mu_{resultant} = (\mu_x^2 + \mu_y^2 + \mu_z^2)^{1/2}$
12-10	0.89	1.49	-4.67	4.99
7CB	5.84	1.16	0.53	5.99

Figure 4B.3.6: (a) The DFT optimised energy minimised molecular structure of (a) N1210, (b) magnified image of molecular conformational structure of N1210 with coordinates and dipole-moment (the end alkyl chains are not shown in the figure for clarity), (c) 7CB (d) Schematic representation of alignment of bent-core molecules. The direction of the resultant dipole moment and the large polarizability directions are denoted by **μ** and P, respectively. **μ** and P are mutually perpendicular in materials with $\Delta\varepsilon < 0$ (upper one). Planar alignment of the director with $\Delta\varepsilon < 0$ (lower one).

4B.4.Dielectric investigations of 7CB, mixtures 5M and 7M:

We have studied 7CB and its mixtures 5M and 7M. The temperature dependent variation of dielectric anisotropy for the pure 7CB, 5M and 7M ($\Delta\varepsilon = \varepsilon_{\parallel} - \varepsilon_{\perp}$) is shown in **Figure 4B.4.7.**

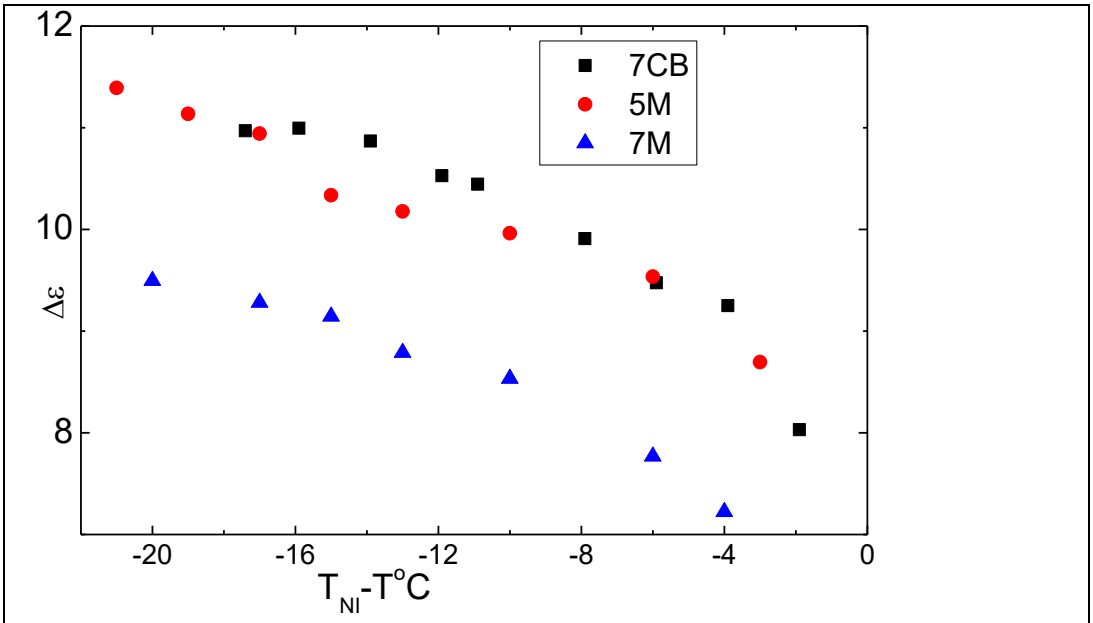

Figure 4B.4.7: Variation of dielectric anisotropy Δε as a function of relative temperature in 7CB, 5M and 7M, f = 1kHz.

The dielectric anisotropy is positive and relatively large and decreases with increasing mol % of bent core compound at a fixed temperature.

The resultant dipole moment (**μ** = 5.99 D) of the 4-n-heptylcyanobiphenyl molecule (DFT optimised structure [28] shown in **Figure 4B.3.6c**) is along the long axis while the bent-core molecules of N1210 possess the dipole moment in a transverse direction. It is apparent from the **Figure 4B.4.7** that the reduction in dielectric anisotropy for 5M is small but for 7M the reduction is larger. However the variation in dielectric anisotropy reflecting the orientational order similar in magnitude suggests that the long axes of the bent-core molecules on an average aligned parallel to the long axes of 7CB molecules as depicted in **Figure 4B.4.8a**.

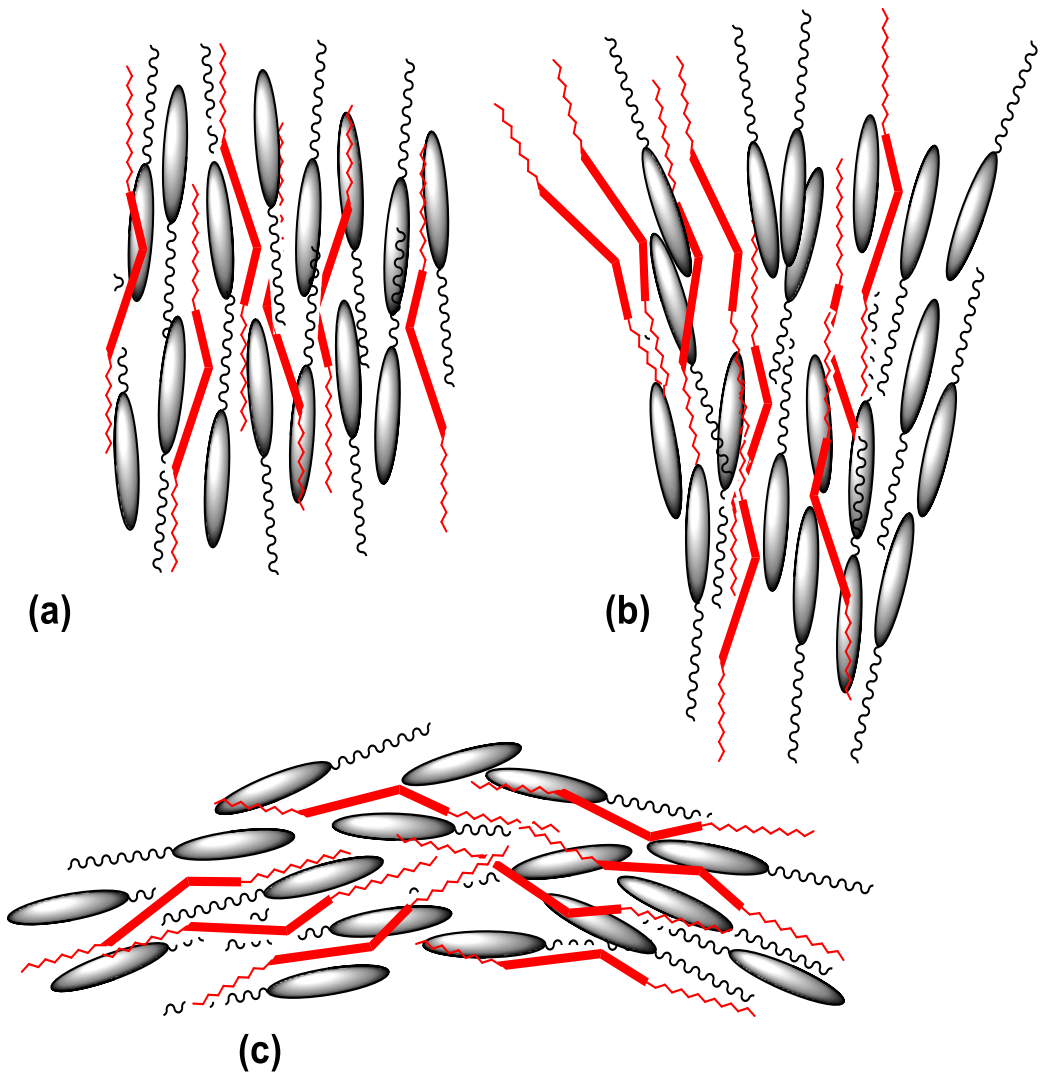

Figure 4B.4.8: (a) Mutual alignment of rod-like and bent-core molecules in nematic phase. Schematic representation of (b) splay and (c) bent distortion of the director in the mixtures.

4B.5.Elastic constants of 7CB, mixtures 5M and 7M:

The capacitance of the empty cell and cell (treated for homogeneous alignment) filled with 7CB, 5M and 7M liquid crystal (LC) materials exhibiting nematic phase only at ambient temperature were determined to evaluate the perpendicular dielectric constant ($\varepsilon_{\perp}$) of the sample. Further the capacitance of LC cell as a function of the applied voltage (0~20V) is measured at different temperatures, which tends to saturate at high voltages (**Figure 4B.5.9**) to estimate the elastic

constants. The measured capacitance value in planar cells at various temperatures far below Fredericksz threshold voltage provided the dielectric constant perpendicular component ($\varepsilon_\perp$). The linear part of the dielectric constant is plotted as inverse function of voltage and fitted it to straight line. The parallel component of the dielectric constant corresponds to $\varepsilon_\parallel$ by extrapolating to 1/V = 0. The splay elastic constant (K_{11}) is obtained from the Fredericksz threshold voltage (V_{th}) of the voltage dependent retardation data from the equation $K_{11} = \varepsilon_o \Delta \varepsilon (V_{th}/\pi)^2$, where $\Delta\varepsilon = (\varepsilon_\parallel - \varepsilon_\perp)$ is the dielectric anisotropy. At strong surface anchoring conditions, the voltages above the threshold voltage V_{th} and the retardation (δ) are given by the parametric equations 1 and 2 [29-31].

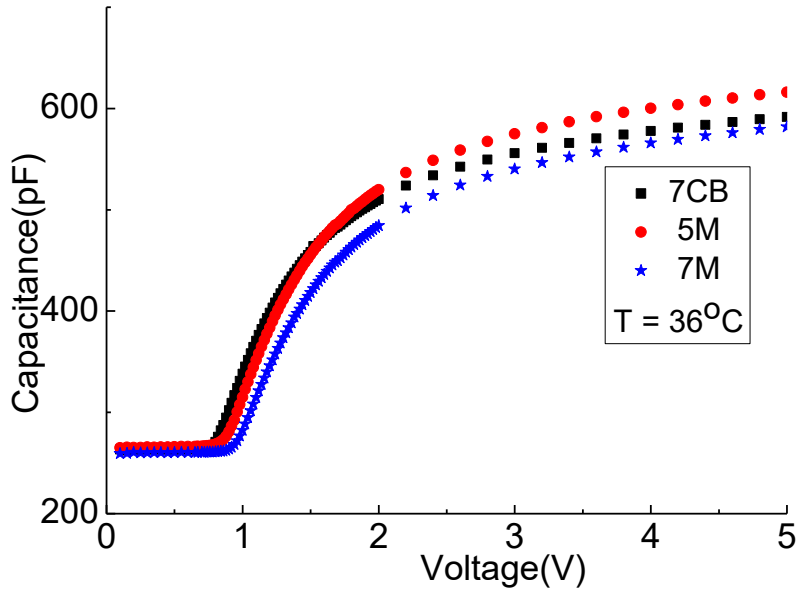

Figure 4B.5.9: Variation of capacitance as a function of voltage for the 7CB , 5M and 7M at T = 36°C, f = 1 kHz

From the critical voltage of the Fredericksz transition we evaluated K_{11} and using this value and substituting other parameters in equation 2 to obtain the best fit of bend elastic constant (K_{33}) was carried out at different temperatures using an iterative procedure.

$$\frac{V}{V_{th}} = \frac{2}{\pi}\sqrt{1+\gamma\sin^2(\phi_m)}$$

$$\int_0^{\frac{\pi}{2}} \sqrt{\frac{1+\kappa\sin^2(\phi_m)\sin^2(\psi)}{(1+\gamma\sin^2(\phi_m)\sin^2(\psi))(1-\sin^2(\phi_m)\sin^2(\psi))}}\,d\psi \quad (1)$$

$$\Delta\phi = 2\pi\frac{n_e d}{\lambda}$$

$$\left(\frac{\int_0^{\frac{\pi}{2}} \sqrt{\frac{(1+\gamma\sin^2(\phi_m)\sin^2(\psi))(1+\kappa\sin^2(\phi_m)\sin^2(\psi))}{(1-\sin^2(\phi_m)\sin^2(\psi))(1+\nu\sin^2(\phi_m)\sin^2(\psi))}}\,d\psi}{\int_0^{\frac{\pi}{2}} \sqrt{\frac{1+\gamma\sin^2(\phi_m)\sin^2(\psi))(1+\kappa\sin^2(\phi_m)\sin^2(\psi))}{((1-\sin^2(\phi_m)\sin^2(\psi))}}\,d\psi} - \frac{n_o}{n_e} \right) \quad (2)$$

Where d is the cell thickness, ϕ_m is the tilt angle at the middle of the cell, $\gamma = ((\varepsilon_{\parallel}/\varepsilon_{\perp}) - 1))$, $\kappa = ((K_{33}/K_{11})-1)$ and $\nu = ((n_e^2/n_o^2)-1)$ and $\sin(\phi) = \sin(\phi_m)\sin(\psi)$.

The temperature-dependent variation of splay (K_{11}) and bend (K_{33}) elastic constants are displayed in **Figure 4B.5.10(a) and Figure 4B.5.10(b)** respectively. K11 increases with decreasing temperature in the nematic phase and exhibited a very little change of curvature. The value of K_{11} monotonically increases with the decreasing temperature. Interestingly there is no significant change in K_{11} variation with temperature in pure 7CB and 5M. However, the variation of K_{11} with temperature for 7M is similar but with decreased magnitude at any relative temperature. The bent-shape of the BLC molecules which are aligned with the rod like 7CB molecules as shown **Figure 4B.4.8a** in nematic phase lowered the splay elastic constant K_{11} [21]. We did not observe any splay distortion of the nematic director (**Figure 4B.4.8b)** caused by BLC molecules in binary mixtures as reported earlier [19].

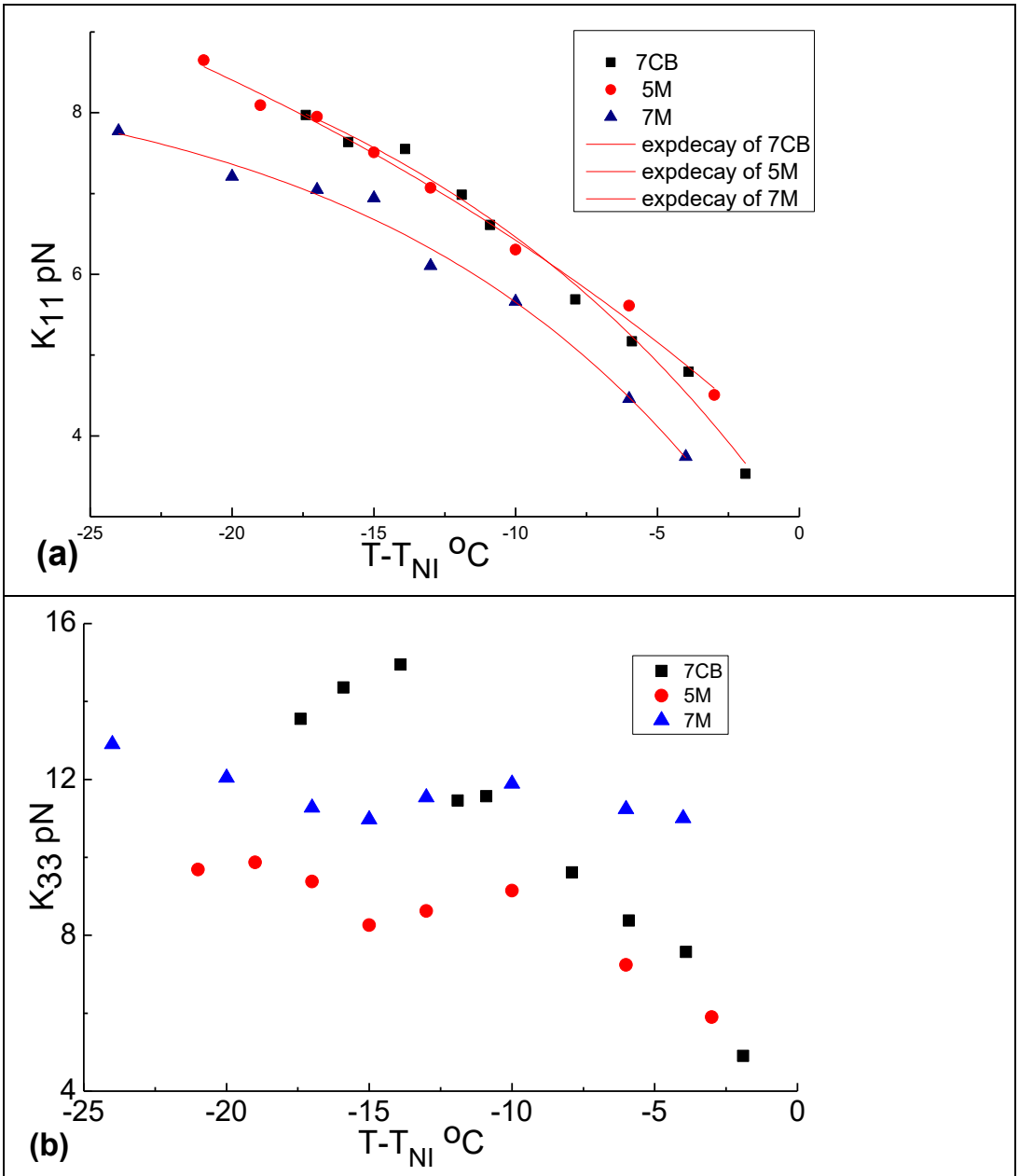

Figure 4B.5.10: Variation of (a) splay and (b) bend elastic constants of pure 7CB and two mixtures 5M and 7M on the relative temperature scale

The bend elastic constant K_{33} decreases significantly with decreasing temperature in 5M when compared to the variation of K_{33} with temperature in pure 7CB (**Figure 4B.5.10b)**. In 5M mixture, the K_{33} increases with decrease of temperature in the nematic region initially followed by a small reduction as the temperature is lowered, and again increases close to room temperature. In case of 7M a small but noticeable increase in K_{33} initially followed by a small reduction

as the temperature is lowered and then increased. Similar anomalous decrease was also reported [19] in mixtures of 8OCB and bent core compound but at a higher concentration only. The sharp reduction in K_{33} with decreasing temperature has to be attributed to shape of the molecule which is now oriented as shown in **Figure 4B.4.8c** in the medium with an increased bend distortion. The bent-shaped molecule consists of two rods with one of the arms longer than the other arm. We assume that the ubiquitous contribution from end alkyl chains towards bend distortion is comparatively smaller than the bent shape of the molecule and therefore is not expected to account for the significant changes observed in K_{33} as the temperature is lowered. Hence if one assumes the interaction between the rod-like biphenyl molecules and the arms of the bent core molecules is significant, then we can consider strong hard-core interactions between the molecules. The increase in probability of orientations that contribute to the decrease of bend elastic constant is dependent on the order parameter. The order parameter describes the extent of mutual alignment of bow-string of bent-core molecules and long axes of 7CB molecules as shown in **Figure 4B.4.8c**. Hence the decrease of bend elastic constant (K33) is due to the strong coupling of the bent shape of the bent-core molecules with bent distortion of nematic director and their alignment with that of 7CB molecules. The variation of K_{33} with decreasing temperature for 7M is distinctly different from what we observed for pure 7CB and 5M. Further analysis is in progress to explain the anomaly in K_{33} for this 7M mixture.

4B.6.Conclusion:

We observed spontaneous periodic stripe domains in nearly homeotropically aligned nematic liquid crystal in Nx phase (1.8^{o}C) above smectic C phase in a four-ring bent core compound. The Nx phase was found to depend on UV-visible light. A small percentage of bent-core molecules in 7CB do not influence the magnitude of dielectric anisotropy but an increase in concentration of bent core molecules (7M) had shown a decrease in dielectric anisotropy. We measured the splay and bend elastic constants in mixtures of rod-like and achiral bent-core four-ring molecules. It indicates that the bow axes are aligned parallel to long axes of rod-like molecules. Similar trend had been observed in splay elastic

constant variation with temperature. However the bend elastic constant had shown an anomalous behaviour. Further detailed investigations are in progress in other four-ring bent core systems exhibiting positive and negative dielectric anisotropies.

References:

[1] T. Niori, T. Sekine, J. Watanabe, T. Furukawa and H. Takezoe, J. Mater. Chem., **6**, 1231-1233, (1996).

[2] D. R. Link, G. Natale, R. F. Shao, J. E. Maclennan, N. A. Clark, E. Korblova and D. M. Walba, Science, **278**, 1924-1927, (1997).

[3] (a) H. Takezoe and Y. Takanishi, Jpn. J. Appl. Phys., **45**, 597-625, (2006); (b) R. A. Reddy and C. Tschierske, J. Mater. Chem., **16**, 907–961, (2006); (c) M. B. Ros, J. L. Serrano, M. R. de la Fuente and C. L. Folcia, J. Mater. Chem., **15**, 5093-5098, (2005); (d) C. Tschierske and G. Dantlgraber, Pramana, **61**, 455-481, (2003); (e) G. Pelzl, S. Diele and W. Weissflog, Adv. Mater., **11**, 707–724, (1999).

[4] (a) C. Tschierske and D. J. Photinos, J. Mater. Chem., **20**, 4263-4294, (2010); (b) M. Lehman, Liq. Cryst. Today, **18**, 31-34 , (2009); (c) V. Gortz, Liq. Cryst. Today, **19**, 37-48, (2010).

[5] E. T. Samulski., Liq. Cryst., **37**, 669-678, (2010).

[6] C. Keith, A. Lehmann, U. Baumeister, M. Prehm and C. Tschierske, Soft Matter, **6**,1704-1721, (2010).

[7] O. Francescangeli, and E. T. Samulski, Soft Matter, **6**, 2413-2420, (2010).

[8] O. Francescangeli,, F. Vita, C. Ferrero, T. J. Dingemans and E. T. Samulski, Soft Matter, **7**, 895-901, (2011).

[9] T. J. Dingemanns, L. A. Madsen, N. A. Zafiropoulos, W. Lin and E. T. Samulski, Philos. Trans. R. Soc. London, Ser. A, **364**, 2681-2696, (2006).

[10] O. Francescangeli, V. Stanic, S. I. Torgova, A. Strigazzi, N. Scaramuzza, C. Ferrero, I. P. Dolbnya, T. M. Weiss, R. Berardi, L. Muccioli, S. Orlandi, and C. Zannoni, Adv. Funct. Mater., **19**, 2592-2600, (2009).

[11] G. Shanker, C. Tschierske, Tetrahedron, **67**, 8635-8638, (2011).

[12] G. Shanker, M. Nagaraj, A. Kocot, J. K. Vij, M. Prehm.and C. Tschierske, Adv. Funct. Mater. **22**, 1671-1683, (2012).

[13] S. J. Pikin, T. J. Dingemans, L. A. Madsen, O. Francescangeli and E. T. Samulski., Liq. Cryst., **39**,19-23, (2012).

[14] W. Weissflog , U. Dunemann, S. F. Tandel, M. G. Tamba, H. Kresse, G. Pelzl, S. Diele, U. Baumeister, A. Eremin, S. Stern and R. Stannarius, Soft Mater, **5**, 1840-1847, (2009).

[15] K. M. Fergusson and M. Hird , J.Mater. Chem., **20**, 3069-3078, (2010).

[16] R. Deb, R. K. Nath, M. K. Paul, N. V. S. Rao, F. Tuluri, Y. Shen, R. Shao, D. Chen, C. Zhu, I. I. Smalyukh and N. A. Clark, J. Mater. Chem., **20**, 7332-7336, (2012).

[17] D. K. Yoon, R. Deb, D. Chen, E. Korblova, R. Shao, K. Ishikawa, N. V. S. Rao, D. M. Walba, I. I. Smalyukh and N. A. Clark, Proc. Nat. Acad. Sci., **107**, 21311-21315, (2010).

[18] R. Pratibha, N. V. Madhusudana and B. K. Sadashiva Science, **288**, 2184-2187, (2000).

[19] B. Kundu, R. Pratibha and N. V. Madhusudana, Phys. Rev. Lett., **99**, 247802, (2007).

[20] B. Kundu, A. Roy, R. Pratibha and N. V. Madhusudana, Appl. Phys. Lett., **95**, 08190218, (2009).

[21] M. R. Dodge, C. Rosenblatt, R. G. Petschek, M. E. Neubert and M. E. Walsh, Phys. Rev. E: Stat. Phys., Plasmas, Fluids, Relat. Interdiscip. Top., **62**, 5056, (2000).

[22] M. R. Dodge, R. G. Petschek, C. Rosenblatt, M. E. Neubert and M. E. Walsh, Phys. Rev. E: Stat. Phys., Plasmas, Fluids, Relat. Interdiscip. Top., **68**, 031703, (2003).

[23] K. Takekoshi, K. Ema, H. Yao, Y. Takanishi, J. Watanabe and H. Takezoe, Phys. Rev. Lett., **97**, 197801, (2006).

[24] L. Chakraborty, N. Chakraborty, D. D. Sarkar and N. V S Rao, S. Aya, K. V. Le, K. Ishikawa and H. Takezoe (unpublished work)

[25] V. M. Pergamenshchik, I. Lelidis, and V. A. Uzunova, Phys. Rev. E: Stat. Phys., Plasmas, Fluids, Relat. Interdiscip. Top., **77**, 041703, (2008).

[26] I. Lelidis and G. Barbero, Europhys. Lett., **61**, 646-652, (2003).

[27] G. Barbero, I. Lelidis and A. K. Zvezdin, Phys. Rev. E: Stat. Phys., Plasmas, Fluids, Relat. Interdiscip. Top., **67**,061710, (2008).

[28] Gaussian 09, Revision B.01,M. J. Frisch, G. W. Trucks, H. B. Schlegel, G. E. Scuseria, M. A. Robb, J. R. Cheeseman, G. Scalmani, V. Barone, B. Mennucci, G. A. Petersson, H. Nakatsuji, M. Caricato, X. Li, H. P. Hratchian, A. F. Izmaylov, J. Bloino, G. Zheng, J. L. Sonnenberg, M. Hada, M. Ehara, K. Toyota, R. Fukuda, J. Hasegawa, M. Ishida, T. Nakajima, Y. Honda, O. Kitao, H. Nakai, T. Vreven, J. A. Montgomery, Jr., J. E. Peralta, F. Ogliaro, M. Bearpark, J. J. Heyd, E. Brothers, K. N. Kudin, V. N. Staroverov, T. Keith, R. Kobayashi, J. Normand, K. Raghavachari, A. Rendell, J. C. Burant, S. S. Iyengar, J. Tomasi, M. Cossi, N. Rega, J. M. Millam, M. Klene, J. E. Knox, J. B. Cross, V. Bakken, C. Adamo, J. Jaramillo, R. Gomperts, R. E. Stratmann, O. Yazyev, A. J. Austin, R. Cammi, C. Pomelli, J. W. Ochters R. L. Martin, K. Morokuma, V. G. Zakrzewski, G. A. Voth, P. Salvador, J. J. Dannenberg, S. Dapprich, A. D. Daniels, O. Farkas, J. B. Foresman, J. V. Ortiz, J. Cioslowski, and D. J. Fox, Gaussian, Inc., Wallingford CT, (2010).

[29] H. J. Deuling, Mol. Cryst. Liq. Cryst., **19**,123-131, (1972).

[30] S. W. Morris, P. Palffy, and D. A. Balzarini, Mol. Cryst. Liq. Cryst., **139**, 263-280, (1986).

[31] G. Barbero and L. R. Evangelista, An Elementary Course on the Continuum Theory for Nematic Liquid Crystals, World Scientific, Singapore, (2000).

Chapter IV

Results and Discussion

Part C

Conformation of nematic phase by electric field, magnetic field and free standing film studies.

4C.1.Introduction:

Since the prediction of a biaxial nematic phase (N_b) by Freiser in 1970,[1] this subject has continued to attract significant interest among scientists during the past decade for reasons of advancing fundamental science and its potential for use in displays. The switching mode in *Nb* is more likely to realize faster response[2,3] and wider viewing angles. For modes such as Vertical Alignment (VA), In-Plane Switching (IPS), Twist Nematic (TN), and Optically Compensated Bend (OCB) using conventional *Nu* to achieving wider viewing angle displays, it is necessary to use expensive optical compensation films[4,5].

The most plausible structure for N_b device to realize both fast response and wider viewing angle is the homeotropically aligned cell with an in-plane switching of the minor director[2]. Lee *et al.*[6] reported fast switching of the minor director with bent core liquid crystal (LC), ODBP-Ph-C7, confirmed already by NMR and x-ray experiments,[10,11] but results of Lee at were strongly criticized by Stannarius for their incorrect interpretation.[7] Recently Le *et al.*[8] reported optical study of the bent core LC, A131, which was confirmed as showing biaxiality in its nematic phase. However, they did not find any evidence of the optical biaxiality in this material[9].

Optical studies like free standing film suggests that the absence of disclinations of unit strength,$|s| = 1$, in the nematic schlieren texture is evidence of biaxiality in the phase [12].

Application of electric field induces eletro-convection patterns in the nematic phase due to hydrodynamic instabilities [13].

4C.2.Results and Discussion:

The appearance of schlirien texture in perfectly homeotropically aligned cell coated by JALS-204, or Cytope, or SE-1211, or silane coupling gives the indication of the presence of secondary director, i,e, presence of biaxiality in the nematic phase. Compound under investigation along with transition temperatures is shown in **Figure 4C.2.1**.

The homeotropic and planar aligned cells are shown in **Figure. 4C.2.2**.

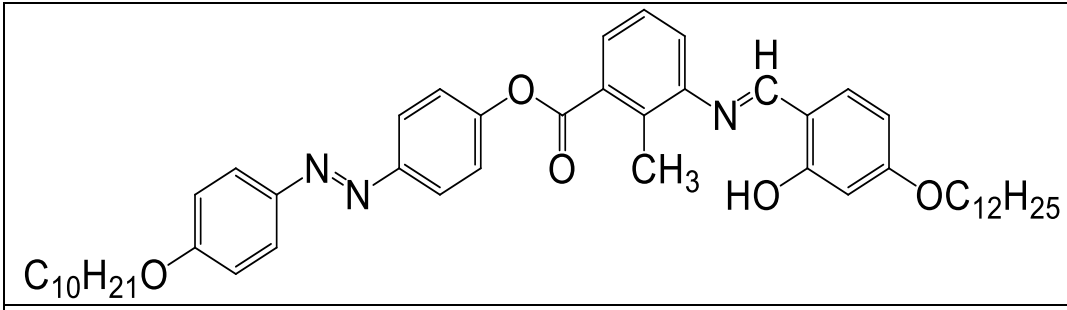

Figure 4C.2.1: Chemical structure of the compound 12-10**.**

12-10: Iso 148.9^{o}C N 135.0^{o}C N_{cybC} 125.3^{o}C Nx 123.5^{o}C SmC 92.9^{o}C Cr

For demonstrating the in-plane switching, a homeotropic cell is used. Both glass plates of the cell are spin coated on the inside with JALS-204 for homeotropic alignment. We prepared two different homeotropic cells: with and without rubbing. The rubbing direction lies at an angle of approximately 45° with respect to the two electrodes for the in-plane switching. In order to align the minor directors, we weakly rub the homeotropic cell as there can be an inhomogeneous distribution of the minor directors.

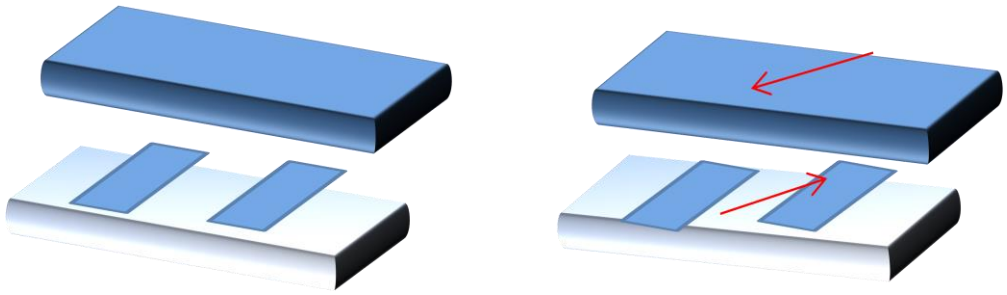

(a) **(b)**

Figure 4C.2.2. Configurations of cells used in optical study (a) homeotropic cell, cell gap=5 µm, (b) homeotropic cell, antiparallel rubbing, cell gap= 5µm. Arrows point to the rubbing direction.

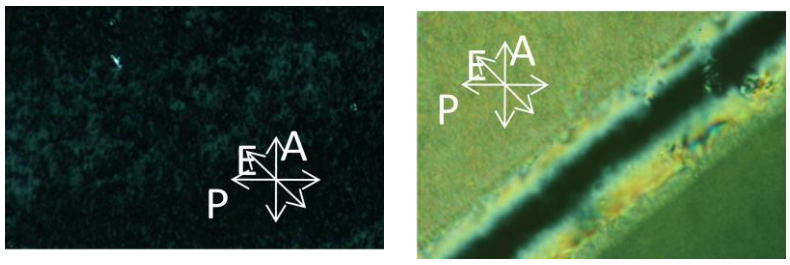

(a) **(b)**

Figure 4C.2.3: Textures of the unrubbed homeotropic cell for temperatures of 135^0C, cell gap = 5µm, (a) E=0Vpp and (b) E= 150Vpp, 1 kHz square wave, A denotes analyzer, P denotes polariser, E denotes electric field.

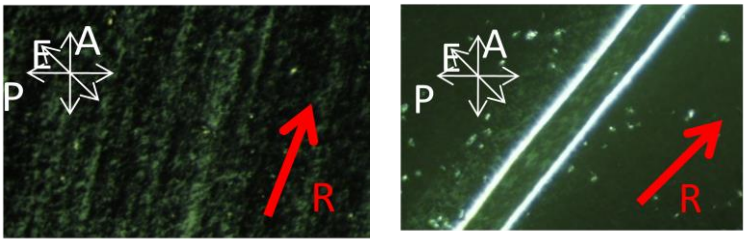

(a) **(b)**

Figure 4C.2.4: Textures of the rubbed homeotropic cell for temperatures of 135^0C, cell gap = 5µm, (a) E=0Vpp and (b) E= 150Vpp, 1 kHz square wave, A denotes analyzer, P denotes polariser, E denotes electric field and R denotes the rubbing direction.

On applying the in-plane electric field of upto150Vpp/µm,at 1kHz square wave, no change in birefringence is observed and also in weakly rubbed cell, on applying the same electric field, the region between the electrodes gets darker which indicates that the director is normal to the in-plane electric field and consequently to the surface of the electrodes. In the absence of electric field, the minor director aligns along the rubbing direction (**Figure. 4C.2.3a** and **4a**). On the application of electric field of upto 150 V/µm, no rotation of the minor director towards the direction of the field (**Figure. 4C.2.3b** and **4b**) is observed, which indicates that the nematic phase is uniaxial in nature.

On applying the magnetic field of strength of B=0.386T, the same phenomenon of decrease of birefringence is observed (**Figure. 4C.2.5**).

The same phenomenon of decrease in birefringence was observed on applying the in-plane electric field in IPS cell with Al spacer (**Figure 4C.3.6**), which gives the indication of the uniaxial nematic phase.

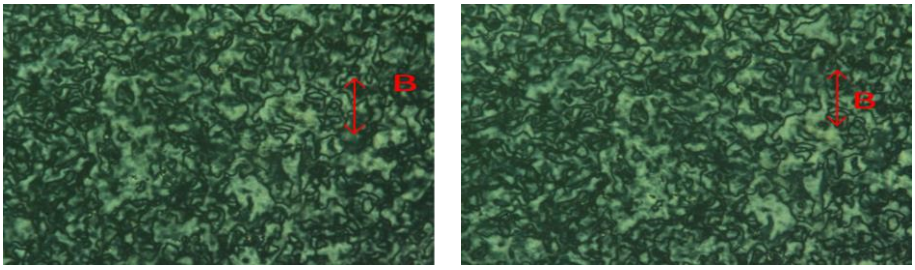

(a) **(b)**

Figure 4C.2.5: Textures of homeotropic alignment of molecules at temperature of 135^0C, (a) with and (b) without magnetic field, arrow denotes the direction of magnetic field.

4C.3.Electric field study in Al spacer-IPS cell:

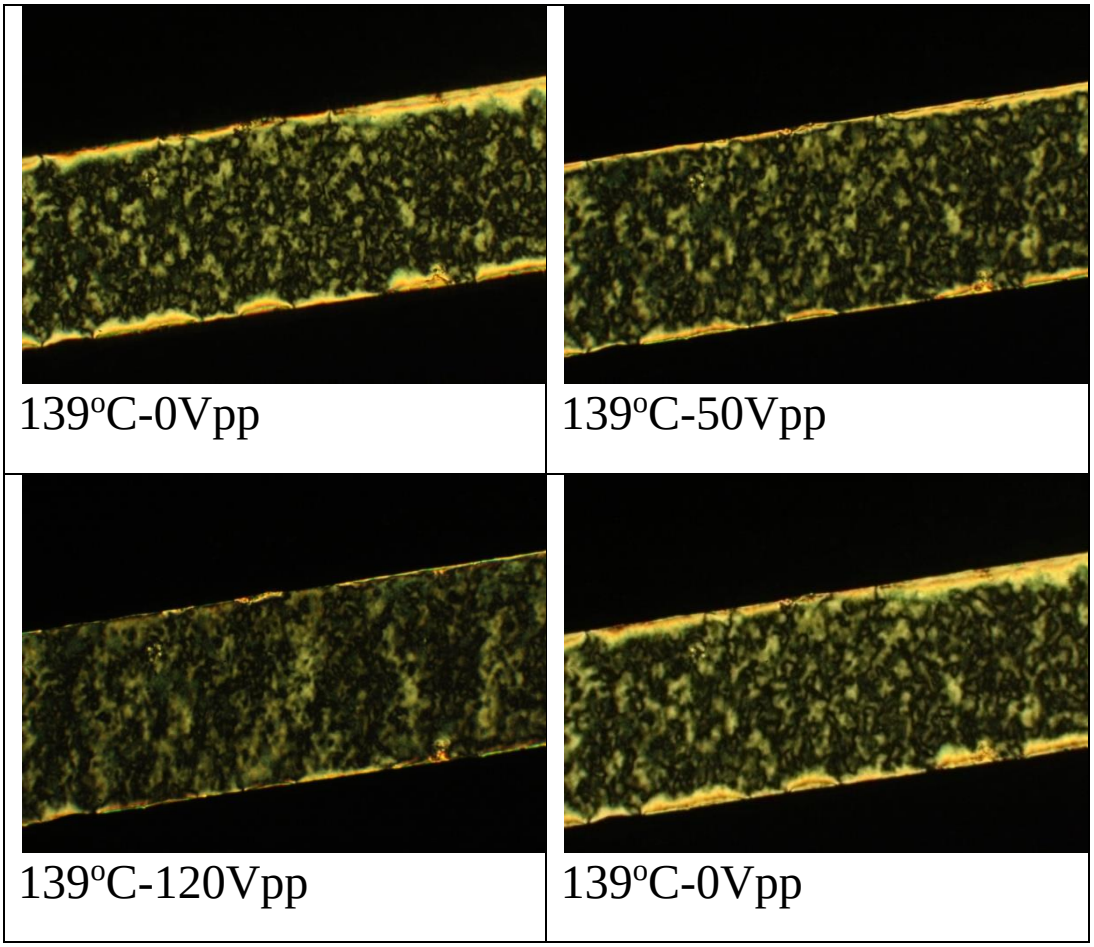

Figure 4C.3.6: Textures of homeotropic alignment of molecules in Al spacer-IPS cell.

4C.4.Electric field in HT cell:

The sample was filled in a homeotropically aligned cell of 6μm thickness in the isotropic phase.With the application of voltage in the nematic phase, domain with

equidistant stripes appear predominately but coming down to the temperature at which the stripe patterns appear, the reverse phenomenon is observed

 **140C,0Vrms,20X**	 **140C,5Vrms,20X**	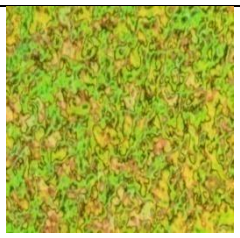 **140C,10Vrms,20X**	 **140C,20Vrms,20X**
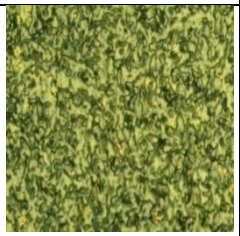 **140C,EFW,20X**	 **122.5C,0Vrms,20X**	 **122.5C,10Vrms,20X**	 **122.5C,EFW,20X**

Figure 4C.4.7: Effect of electric field in the nematic phase in homeotropic alignment of molecules.

4C.5.Free standing film study:

Free standing films were prepared by spreading the fluid over a circular hole, less than about 1mm in diameter, drilled in an aluminium plate. With a film of this thickness, the influence of nematic-air interface on the orientational order in the bulk of the sample may be expected to be quite small. Large 4-brush disclinations $|s| = 1$ appeared readily in the uniaxial Nu films as shown in **Figure 4C.5.9**.

Nematic fluid in a droplet of glycerol was also observed under polarising microscope, where 4-brush disclinations $|s| = 1$ appeared in the uniaxial nematic phase **Figure 4C.5.8**.

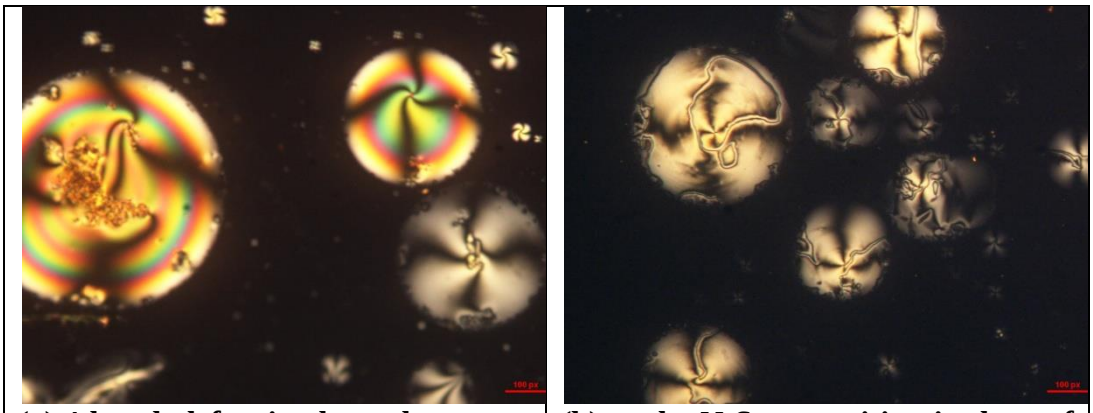

(a) 4-brush defect in glycerol | **(b) at the N-Sm transition in drop of glycerol**

Figure 4C.5.8: Textures of nematic phase in droplets of glycerol.

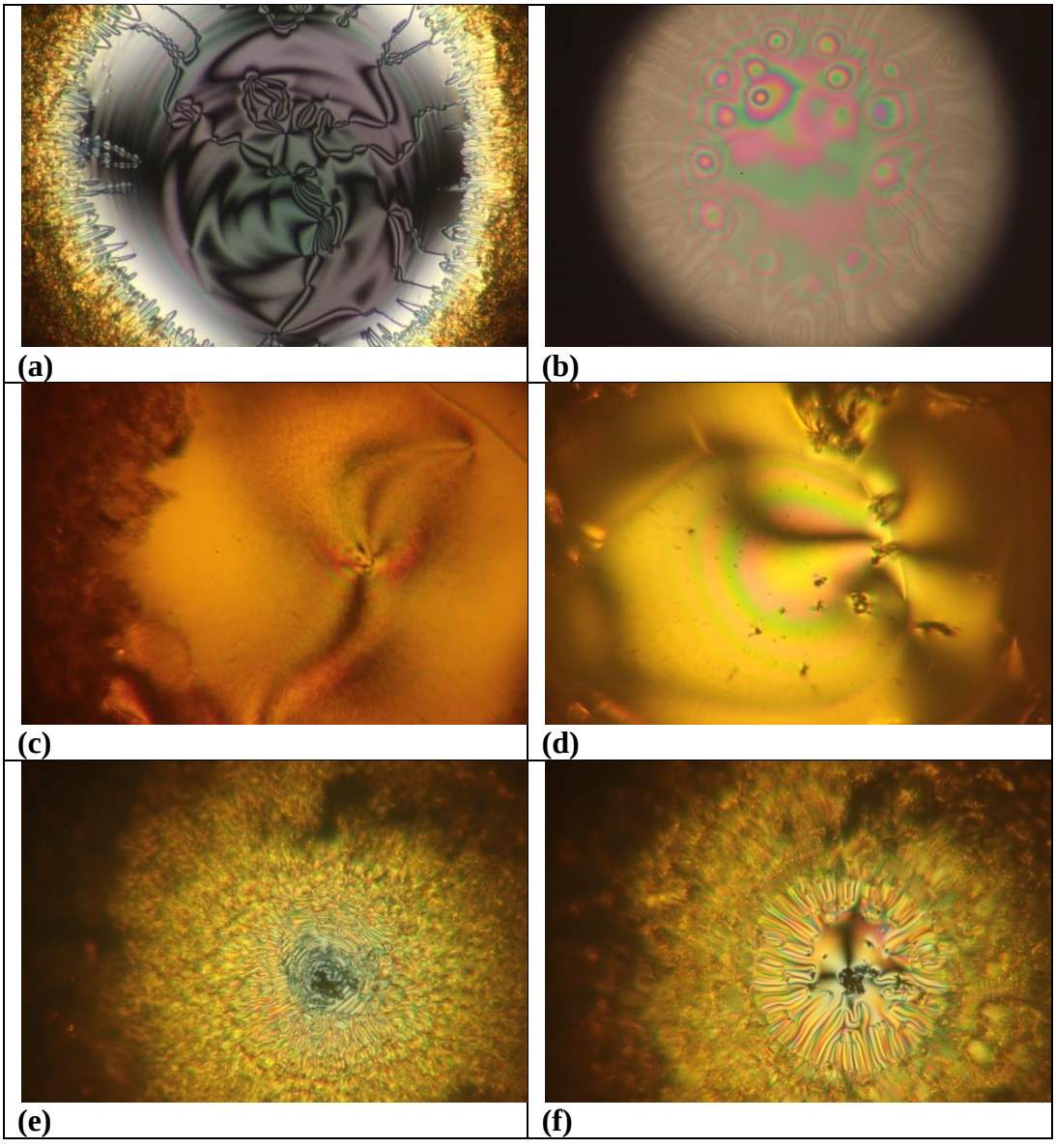

(a) | **(b)**

(c) | **(d)**

(e) | **(f)**

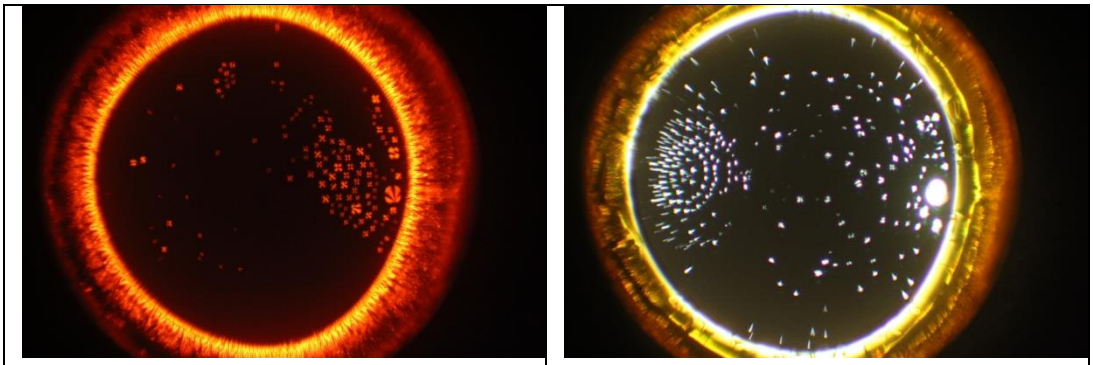

(g) red filter inserted **(h)**

Figure 4C.5.9: Free standing film textures of 12-10 in a plate with hole of 1mm diameter; (a) 140^{o}C, film of less thickness, 4-brush defects (uv power of 154μW/cm^{2}) (b) 140^{o}C, combined with reflectance mode (c) 4-brush defects at 130^{o}C (d) film of maximum thickness at 130^{o}C (e) N-SmC transition (f) after transition at SmC, 120^{o}C, (g) induced N-Sm transition. (h) Strong UV power (1925μW/cm^{2}).

4C.6.Conclusion:

On applying the in-plane electric field in unrubbed and rubbed cell, no change in birefringence is observed which indicates the nematic is uniaxial in nature. On application of magnetic field also, no change in birefringence is observed. Free standing film study in glycerol and air produces schlierien texture with 4- brush defects only which reveals that the nematic phase is uniaxial in nature. Electric field in homeotropic cell produces pre-wavy patterns which produces question of whether ferroelectric switching is present or not.

References:

[1] M. J. Freiser, *Phys. Rev. Lett*. **24**, 1041,(1970).

[2] G. R. Luckhurst, *Thin Solid Films* **393**, 40,(2001).

[3] R. Berardi, L. Muccioli, and C. Zannoni, *J. Chem. Phys.* **128**, 024905 (2008).

[4] H. Mori and P. J. Bos, SID Int. Symp. Digest Tech. Papers **29**, 830, (1998).

[5] J. Chen, K. -H. Kim, J. -J. Ryu, J. H. Souk, J. R. Kelly, and P.J. Bos, SID Int. Symp. Digest Tech. Papers **29**, 315,(1998).

[6]J. Lee, T.-K. Lim, W.-T. Kim, and J. Jin, *J. Appl. Phys.* **101**, 034105, (2007).

[7] R. Stannarius, *J. Appl. Phys.* **104**, 036104, (2008).

[8] V. Prasad, S.-W. Kang, K. A. Suresh, L. Joshi, G. Wang, and S. Kumar, *J. Am. Chem. Soc*. **127**, 17224, (2005).

[9] K. V. Le, M. Mathews, M. Chambers, J. Harden, Q. Li, H. Takezoe, and A. Jákli, *Phys. Rev. E* **79**, 030701(R), (2009).

[10] L. A. Madsen, T. J. Dingemans, M. Nakata, and E. E. Samulski, *Phys. Rev. Lett.* **92**, 145505, (2004).

[11] B. R. Acharya, A. Primak, and S. Kumar, *Phys. Rev. Lett.* **92**, 145506, (2004).

[12] Chandrasekhar, S., Geetha Nair, G., Praefcke, K., and Singer, D., *Mol. Cryst. liq. Cryst*., **288,** 7, (1996).

[13] G. Shanker, M. Nagaraj, A. Kocot, J. K. Vij, M. Prehm.and C. Tschierske, *Adv. Funct. Mater.* **22**, 1671-1683, (2012).